Chapter 3

APPLICATIONS OF MODULATED TEMPERATURE DIFFERENTIAL SCANNING CALORIMETRY TO POLYMER BLENDS AND RELATED SYSTEMS

Douglas J. Hourston and Mo Song
IPTME, Loughborough University, Loughborough LE11 3TU, UK

1 Introduction

The characterisation of multi-component polymer materials [1] has been pursued vigorously in recent years. Many types of such materials (including polymer blends, block copolymers, structured latexes and interpenetrating polymer networks) are now commercially available [2,3] and their ever better characterisation remains important. It is necessary to obtain morphological parameters such as the thickness and weight fraction of interfaces/interphases[1] and to understand the relationships between morphology and mechanical properties of such multi-component polymeric materials [2–8]. A common feature across the spectrum of multi-component polymeric materials is the presence of interfaces [2,5,7,8]. The properties of the interface are invariably central to the properties of the composite and the ability to understand and optimise the interface is recognised as a key feature in the development of improved polymeric materials. Most polymer pairs are immiscible [5,6]. Thus, the majority of blends are two-phase and their morphology depends on the type of molecular interaction, the rheology of the components and the processing history. Models used to describe

[1]The term interface implies a two-dimensional structure. It is clear in nearly all practical cases in polymer science that the regions between phases are three-dimensional in nature. These regions are also often likely not to be isotropic, but of a compositionally graded nature which means they do not meet the strict definition of a phase. In this chapter, the terms interface and interphase will be used essentially interchangeably.

M. Reading and D. Hourston (eds.), Theory and Practice of Modulated Temperature Differential Scanning Calorimetry, 161–216.

multi-component materials show that certain properties can be correlated with the interphase volume fraction [7,8]. Many techniques have been used to characterise the morphology of multi-phase polymeric materials. Porod's analysis [9] of small-angle X-ray (SAXS) and neutron scattering (SANS) data has been used to estimate interfacial thickness and domain size [10,11]. Dynamic mechanical thermal analysis (DMTA) data have been modelled [12] by assuming interfacial profiles. A technique that can yield both interfacial thickness and composition gradient across the interface is transmission electron microscopy (TEM) [10]. Results that are in good agreement with SAXS and DMTA [12] have been obtained for highly ordered systems, such as ABA-type block copolymers.

In the characterisation of the morphology of multi-component polymeric materials, the glass transition temperature, the composition distribution in the phases, phase size and shape and the thickness and volume (or weight) fraction of the interface are clearly important. DMTA and differential scanning calorimetry (DSC) are suitable for the measurements of the glass transition temperature. It is conventional, simple and rapid to use DSC to study polymer blends. However, because the sensitivity and resolution of DSC are usually not good enough, overlapping thermal events, including T_gs from pure phases and any interface resulting from partial miscibility, cannot usually be separated [13,14].

A basic limitation exists on the use of glass transition determinations in ascertaining the extent of polymer–polymer miscibility in blends composed of components which have similar (<15°C difference) T_gs. In these cases, resolution by the DSC technique [5] is not possible. Also, for small concentrations (less than 10%), the transition signal is difficult to resolve [5,15]. Structural relaxation at the T_g [15] can also distort the shape of the transition. Although DSC has been used extensively to characterise IPNs [16–18], it fails when IPNs show complex phase structure. Most researchers have turned to DMTA to observe the transitions in IPNs, for example, because it is more sensitive [1,5,6]. An interesting morphological parameter, the degree of segregation in IPNs can be obtained from DMTA data using Lipatov's method [19]. The DMTA characterisation method developed by Annighofer and Gronskin [12] is only suitable for the study of the morphology of block copolymers with a high degree of orientation. In fact, it is difficult, quantitatively, to obtain either the weight (or volume) fraction of each phase or information on composition distribution in multi-phase polymeric materials from DMTA data. It is always necessary to make some assumptions regarding the nature of the interface.

Microscopies and scattering techniques [10,12] are used to study the micro-domain size, shape and interface content. TEM has been used in many instances in order to determine the miscibility, or phase segregation,

of IPNs. Detailed information about polymer blend morphology can be gained from this technique. This includes information about the continuous phase and the size and shape of the domains and their distribution. At very high magnifications, domains in the order of 1 nm can, in theory, be investigated [20]. The preparation of the samples can sometimes be difficult, since ultra-thin sections have to be cut. Specimen preparation [21] and the interpretation [22], and possible artefacts caused by electron beam [20] and sectioning damage [22] have been described.

It is not difficult to study the micro-domain size and the interfacial thickness of block copolymers using SAXS. The volume fraction of interface in such a multi-phase system [10,12] has been obtained using this technique. However, it is not easy to determine the fraction of interphase in partially miscible, or essentially immiscible, polymer blends. Regarding the application of SAXS to measurements of the morphological parameters of multi-phase polymeric materials, Ruland [23] has fully analysed the experimental difficulties. He indicated that the determination of the width of domain boundaries by the SAXS method can contain substantial errors if the boundary region is not represented by a smooth homogeneous density transition, but by a statistical structure of a certain coarseness. It has been shown that these errors, in general, lead to an under-estimation of the values of the boundary widths in the case of block copolymers. Samples with a highly preferred orientation of the interface planes can be used to minimise the errors and to obtain information on the coarseness of the domain boundaries [23].

Although the existence of a diffuse interfacial region in multi-phase systems has been detected by solid-state NMR spectroscopy [24–27] and by dynamic relaxation measurements [12,28], to date only SAXS and SANS are capable of providing interfacial thickness values. Scattering techniques, especially SANS, are rather specialised and are not widely available. DMTA can be used to study interfaces [12] by assuming interfacial profiles. TEM results [10] from highly ordered systems are in good agreement with SAXS and DMTA [12] data. SANS has been used by McGarey [29] to study IPNs, but IPNs are far from the ideal system for study by this technique.

To help summarise the above discussion, Table 3.1 gives a comparison of the applicabilities of the DSC, DMTA, SAXS, SANS, microscopies and solid-state NMR techniques to the study of multi-component polymeric materials. It can be seen that if one wants to obtain detailed morphological information, several characterisation techniques must be used. It is also obvious that even when the above characterisation techniques are available, one cannot obtain all the morphological parameters such as the weight fraction of each phase and the concentration distribution in multi-phase polymeric materials.

Table 3.1. Comparison of the abilities of various characterisation methods for multi-component polymeric materials

	DSC	SAXS	SANS	DMTA	LM	SEM	TEM	NMR
Resolution (nm)	20	2	1	15	1000	20	1	1
Specimen preparation	Easy	Easy	Difficult	Easy	Easy	Easy	Difficult	Easy
T_g	Quant	No	No	Quant	No	No	No	No
Multi-phase information	Yes	Yes	Yes	Yes	Yes	Yes	Yes	Yes
Interfacial information	Yes*	Yes	Yes	Yes*	No	No	Yes*	Yes
Interfacial thickness	No	Quant	Quant	No	No	No	Qual	No
Weight fraction	Qual	No	No	No	No	No	No	Yes*
Domain size	No	Yes	Yes	No	Yes	Yes	Yes	No

LM: light microscopy; Qual = qualitative; Quant = quantitative.
*Not always possible (1,5,10,26).

It is very desirable to establish widely applicable, and readily available, methods for the characterisation of multi-phase polymeric materials that can overcome the disadvantages of the above techniques.

The possibilities arising from the advent of MTDSC will now be discussed. Complex thermal histories affect the ease with which it is possible to make determinations of the increment of heat capacity, ΔC_p, at T_g because of structure relaxation. If a thermal analysis apparatus that can separate the structure relaxation part from the total heat flow signal can be developed, ΔC_p could be determined accurately. It is well known that ΔC_p is related to the weight fraction of each component in a heterogeneous system such as a polymer blend. In multi-phase polymeric materials, each phase has its own characteristic glass transition temperature and ΔC_p. Thus, important information may be obtained from ΔC_p and glass transition measurements, allowing such materials to be analysed quantitatively.

For pure, fully annealed polymers, the glass transition is approximately symmetrical [5]. For partially miscible systems in which there are interfaces, the transition will be asymmetric and become broadened [5]. This asymmetry and broadening may provide a wealth of information of both practical and theoretical value that has not yet been fully extracted.

Because modulated temperature DSC (MTDSC) can separate overlapping thermal events and separate the total heat flow into two parts: the reversing (proportional to heating rate) and the non-reversing (dependent on temperature) components, it allows the study of the asymmetry and broadening of the glass transition. Important information can be obtained from the differential of heat capacity, dC_p/dT, signal over the glass transition region. Using this signal, multi-component polymeric materials may be analysed quantitatively. In this chapter, we will discuss the dC_p/dT signal and its use in the quantitative characterisation of such materials. The MTDSC technique leads to an improvement in the detection of the glass transition, readily

provides a measure of ΔC_p and indicates the extent of polymer–polymer miscibility. Based on this new signal, symmetric and asymmetric interdiffusion, interface development in bilayer and structured latex films, and the morphology of IPN materials will be discussed.

2 Heat Capacity and its Differential with Temperature Signal Over the Glass Transition Region

In chapter 1, a full theoretical treatment of the behaviour of the MTDSC signals over the glass transition region [30] has been presented.

The following equations arise from this treatment discussed in Chapter 1.

$$C'_p = A + BT + \Delta C_p \big/ \left(1 + \omega^2 \tau_g^2 \exp\left(-2\Delta h^* \big/ \left(RT_g^2\right)(T - T_g)\right)\right) \quad (1)$$

$$C''_p = \Delta C_p \omega \tau_g \exp\left(-\Delta h^* \big/ RT_g^2 (T - T_g)\right) \big/ \left(1 + \omega^2 \tau_g^2 \exp\left(-2\Delta h^* \big/ \left(RT_g^2\right)(T - T_g)\right)\right) \quad (2)$$

Figures 3.1 and 3.2 compare the dC_p/dT versus temperature data from experiments with theoretical data (using the above equations) and a Gaussian function for, respectively, polystyrene and a (50/50 by weight) miscible blend of poly(methyl methacrylate) and poly(styrene-*co*-acrylonitrile) [30]. Clearly, the experimental data can be described by both the theory, and also by a Gaussian function, G, of the glass transition temperature, the width

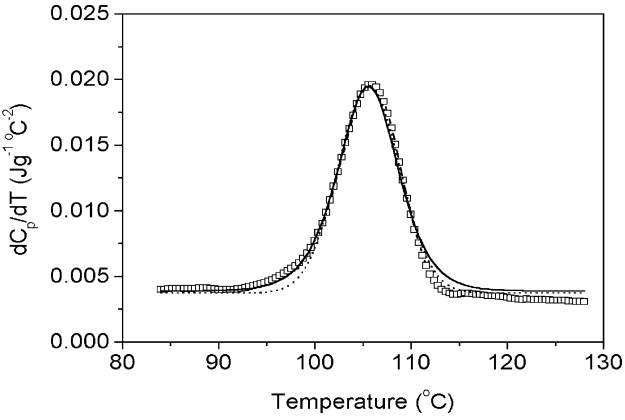

Figure 3.1. Comparison of the dC_p/dT versus temperature data for polystyrene from experiment (square points), theory (solid line) and from the Gaussian function (dots).

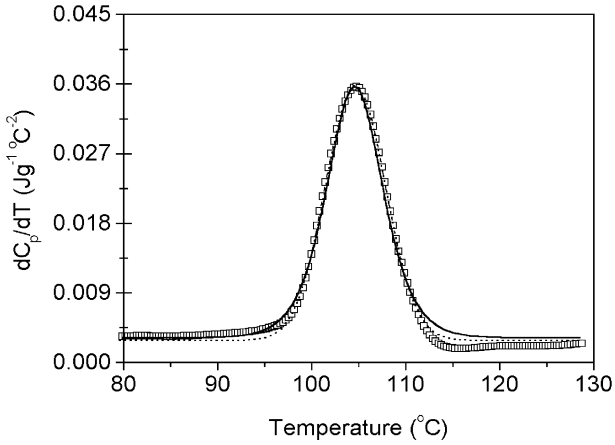

Figure 3.2. Comparison of the dC_p/dT versus temperature data for a PMMA/SAN(50:50) blend from experiment (square points), theory (solid line) and from the Gaussian function (dots).

of the transition at half height, ω_d, the increment of heat capacity and the temperature.

$$G = f(T, T_g, \omega_d, \Delta C_p) = \Delta C_p / \left[\omega_d (\pi/2)^{1/2}\right] \exp\left[-2(T - T_g)^2/\omega_d^2\right] \quad (3)$$

In this chapter, the Gaussian function description of the change of dC_p/dT versus temperature at the glass transition will be used in the analysis of various polymer blend systems. The Gaussian function approach to modelling the glass transition is chosen over theory [30] because in Eq. (1), the τ_g and Δh^* terms are generally unavailable for polymers.

3 Measurements of the Glass Transition Temperature and Increment of Heat Capacity

As mentioned above, the commonly occurring complex thermal histories experienced by polymeric artefacts during manufacture affect the ease with which it is possible to make determinations of the glass transition temperature accurately by conventional DSC. Thermograms with different shapes in the glass transition region often make the conventional extrapolations ambiguous. It is also often the case that the measurement of ΔC_p in the glass transition region is highly subjective, not to mention time-consuming, using conventional DSC.

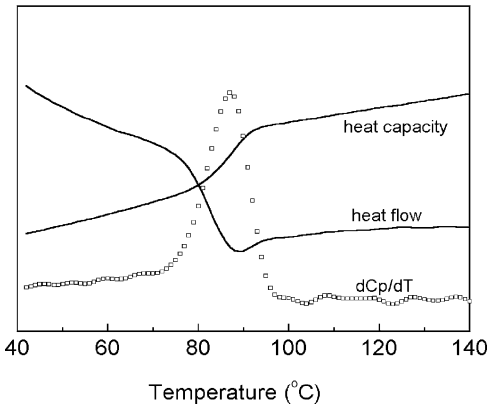

Figure 3.3. Heat flow, heat capacity and dC_p/dT versus temperature data for polystyrene.

Figure 3.3 shows the changes of total heat flow, heat capacity and dC_p/dT with temperature for a PS sample [31]. Because of the effect of thermal history, the relaxation event appears in the total heat flow signal. It can be seen that the peak position of the dC_p/dT versus temperature signal corresponds to the point of inflection of the heat capacity curve between the glassy and liquid states. If the peak position, as is often done for a melting point, is used to determine the T_g, it will be very easy and reproducible to use in subsequent analyses.

Figure 3.4 gives another example of MTDSC output. In this case, data for an interpenetrating polymer network are reported. Obviously, it is very difficult to obtain the T_g values with any accuracy from the total heat flow signal, which is very complex. However, it is very easy, using the dC_p/dT

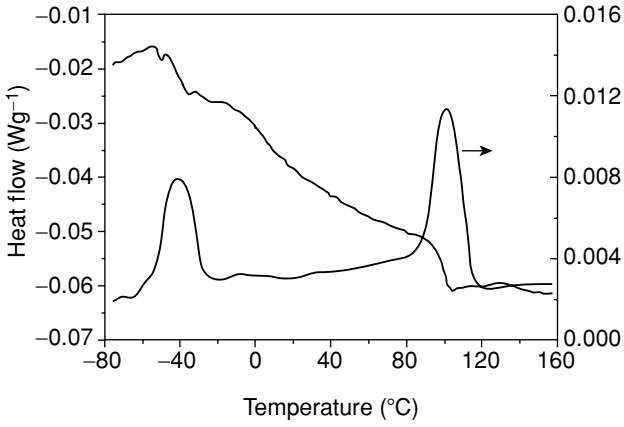

Figure 3.4. Heat flow and dC_p/dT versus temperature data for a polyurethane/polystyrene IPN.

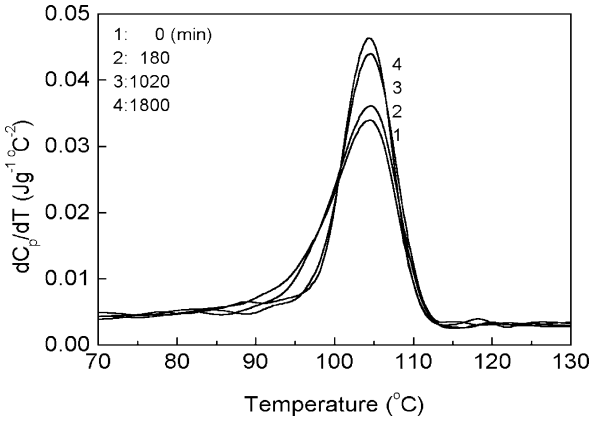

Figure 3.5. dC_p/dT versus temperature data for different annealing times at 80°C for a SAN/PMMA blend (50/50).

signal, to obtain both of these T_gs accurately and simply. Figure 3.5 again shows the change of dC_p/dT with temperature for a PMMA/SAN (50/50, wt/wt) compatible blend [31], but for different annealing times at 80°C. The peak position is almost constant with time. However, the onset point shifts to higher temperature with increasing annealing time. Figure 3.6 gives the result of a heat/cool experiment for polystyrene [31]. The T_g is 85°C on cooling and 86°C on re-heating showing the measurement to be robust. Figure 3.7 gives another example for polystyrene, this time annealed at different temperatures for 1 hour. The T_g was 86 ± 1°C for the different annealing temperatures. Figure 3.8 shows the changes of T_g with annealing time for a polyvinyl acetate sample. With increasing time, the value of T_g

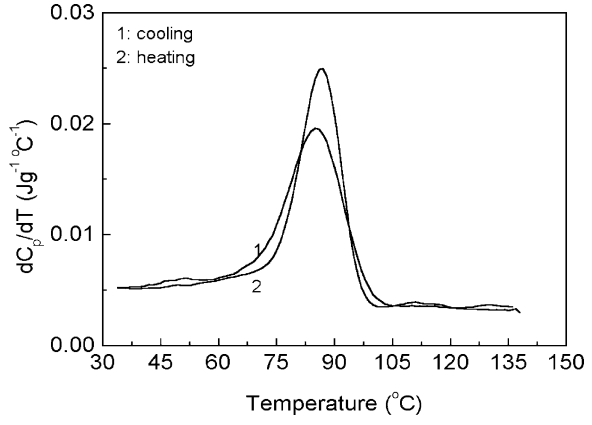

Figure 3.6. dC_p/dT versus temperature data for polystyrene in a cyclic experiment.

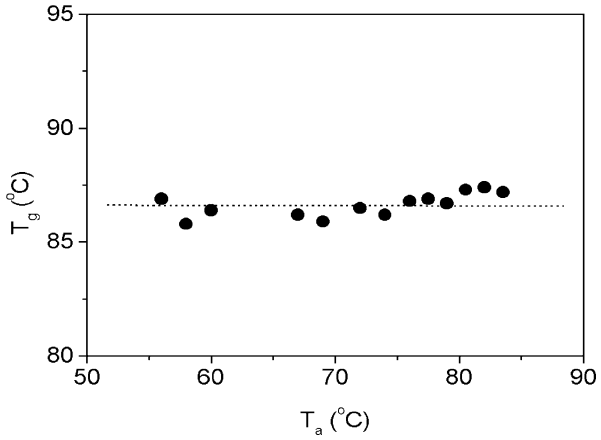

Figure 3.7. T_g versus annealing temperature for polystyrene. Annealing time was 1 h.

increased. However, even for long times, the difference was only 1.6°C. These changes are relatively small. These last few figures illustrate that the dC_p/dT signal is a sensitive, and, therefore, a valuable one with which to probe the glass transition.

For small concentrations of a given component in a polymer blend (less than 10 wt%), the resulting weak transition is typically very difficult to resolve using conventional DSC or DMTA [5,15]. Using MTDSC, T_g determinations were performed [32] on a physical blend containing four components: pure PS plus PPO-30 (a PS/polyphenylene oxide (PPO) blend at a composition ratio of 70/30) plus PPO-70 (a PS/PPO blend at a composition ratio of 30/70) plus pure PPO. The amount of each component was 44.0:7.1:13.4:34.5, by weight. Figure 3.9 shows both the heat capacity and

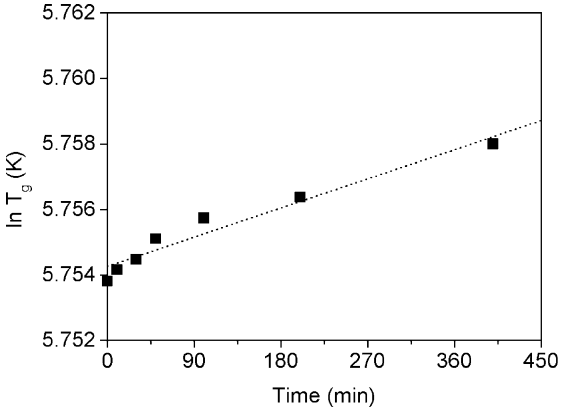

Figure 3.8. ln T_g versus annealing time at 30°C for polyvinyl acetate.

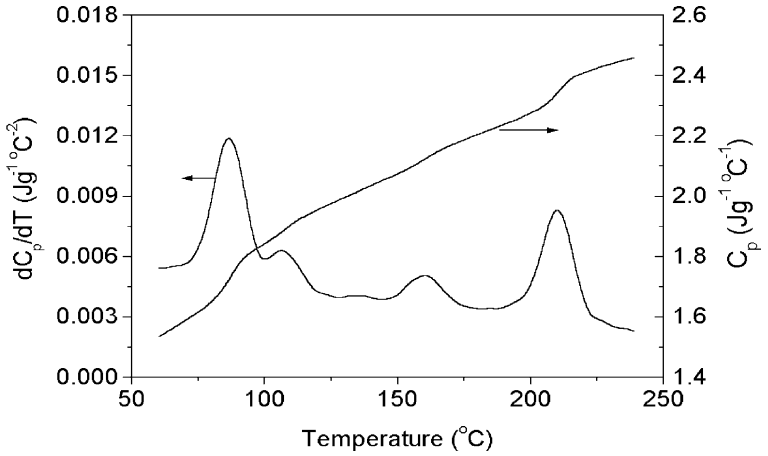

Figure 3.9. dC_p/dT versus temperature data for a PS + PPO-30 + PPO-70 + PPO physical blend.

the dC_p/dT with temperature signals. From the heat capacity signal, not all the transitions are clear. However, four transitions are clearly evident in the dC_p/dT signal, despite the fact that the PPO-30 is only present at 7.1% by weight.

In summary, the dC_p/dT signal is a very useful tool to determine T_g values. The benefits of using dC_p/dT to measure T_g are as follows.

(i) The position and shape of the glass transition are much less affected by thermal history and experimental conditions than is the case with conventional DSC.
(ii) Glass transitions can be represented as Gaussian curves.
(iii) Events such as the loss of small amounts of residual solvent, which can occur when studying blends, affect the reversing signal very little (see Chapter 1), but can have significant effects on the heat flow signal in conventional DSC.
(iv) Resolution is improved in MTDSC because both the step at T_g in the reversing signal is sharper than that in conventional DSC and low underlying heating rates can be used while still retaining a high signal-to-noise ratio in the reversing heat capacity measurement.

The value of apparent heat capacity, C_p^a, (not calibrated) may be written as follows [31].

$$C_p^a = A + BT + f(T) \tag{4}$$

A and B are constants and $f(T)$ is a function of temperature. Outside the glass transition region, $f(T) = 0$. The following relation holds for

the dC_p^a/dT value.

$$dC_p^a/dT = B + df(T)/dT \tag{5}$$

To obtain the required ΔC_p values, it is only necessary to integrate the signal over the region of interest, which in this case is the glass transition.

$$\Delta C_p = \int_{C_p(i)^a}^{C_p(e)^a} \left(dC_p^a/dT\right)dT \tag{6}$$

$C_p(i)^a$ and $C_p(e)^a$ are the initial and final values of the apparent heat capacity in the glass transition region. It is assumed that the integration constant is independent of temperature. The above equation to calculate ΔC_p only needs a one-point calibration for heat capacity selected in the transition region. The reason for this is that if it is assumed that the calibration constant of heat capacity is K_1 at the onset point of the glass transition and is K_2 at the final point, ΔC_p is given as follows.

$$\Delta C_p = K_2 C_p(e)^a - K_1 C_p(i)^a \tag{7}$$

The value of the one-point calibration constant, K, is given approximately by Eq. (8)

$$K = (K_1 + K_2)/2 \tag{8}$$

Consider that

$$K = K_1 + \delta = K_2 - \delta \tag{9}$$

δ is a small increment. Then, Eq. (10) can be rewritten as follows.

$$\Delta C_p = K\left[\Delta C_p^a + \delta/K(C_p(e)^a + C_p(i)^a)\right] \tag{10}$$

Table 3.2 lists how the calibration constants change with temperature. According to the experimental results, it was found that $\delta/K \sim 10^{-3}$. Thus,

$$\Delta C_p = K\,\Delta C_p^a \tag{11}$$

The difference between the results from Eq. (11) and those from Eq. (7) is small. The error resulting from using Eq. (11) is about 3%.

Table 3.2. Change of heat capacity calibration constant with temperature

Temperature (°C)	Calibration constant
36.85	1.1947
56.85	1.1846
76.85	1.1764
96.85	1.1654
116.85	1.1573
136.85	1.1522
156.85	1.1507
166.85	1.1459

There is considerable interest in the values of ΔC_p at the T_g and various generalisations [33,34] have been suggested either for ΔC_p or for the product $\Delta C_p T_g$. ΔC_p measurement is complex and time-consuming by conventional DSC [13,35]. Heat capacity values at T_g from conventional DSC studies have been obtained [36] by extrapolation of the linear equations used to describe the glass and liquid states. Based on the new MTDSC method, the determination becomes very simple and rapid. Later, we will discuss how this makes it a convenient way to analyse multi-phase polymeric materials.

Figures 3.10 and 3.11 show the changes of ΔC_p for PS [31] and for a 50/50 SAN/PMMA blend at different annealing temperatures and for different annealing times, respectively. For the PS sample, the annealing time was 60 min. The results show that the values for PS are almost constant

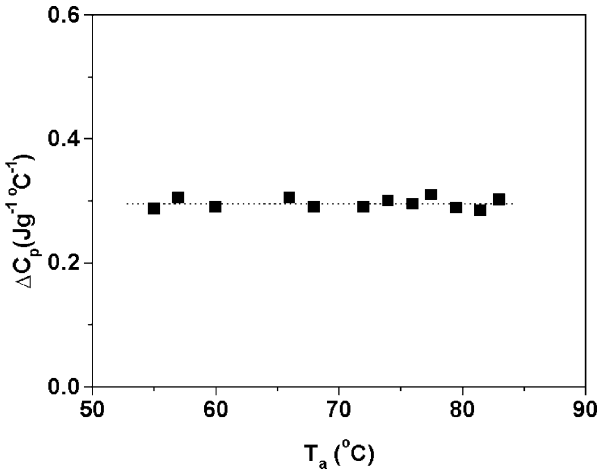

Figure 3.10. ΔC_p versus annealing temperature for polystyrene. Annealing time was 1 h.

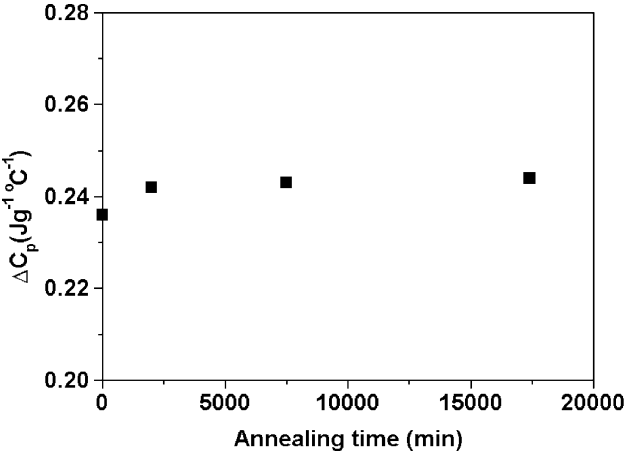

Figure 3.11. ΔC_p versus annealing time at 80°C for an SAN/PMMA blend (50/50 wt/wt).

for these different thermal histories. The average value of ΔC_p is 0.293 $Jg^{-1}\,°C^{-1}$. Comparison with values in the literature [37] indicates that the average difference is about 3%.

4 Multi-Component Polymer Materials

4.1 IMPROVEMENT IN THE MEASUREMENT OF POLYMER–POLYMER MISCIBILITY

Polymer–polymer miscibility is usually characterised [1,5,6] by investigating the optical appearance, morphology, glass transition temperature or the crystalline melting behaviour of the blend [38,39]. A blend of two amorphous polymers with different refractive indices will be judged to be miscible if it is optically clear. Measurement of the glass transition temperature, or temperatures, of a polymer blend is the most convenient and popular way of investigating polymer–polymer miscibility.

T_g is commonly measured by the DSC technique, but the use of T_g determination for studying polymer–polymer miscibility has its limitations. The glass transition region for a given polymer can cover at least a 15°C range [5,15] and often significantly more. Thus, if the difference of the glass transition temperatures between the two polymers in a blend is less than about 15°C, it has been almost impossible to detect the extent of mixing by DSC [5,15].

It is known [6] that poly(styrene-*co*-acrylonitrile), SAN, is miscible with PMMA when the acrylonitrile content is between 10 and 30 wt%. To check

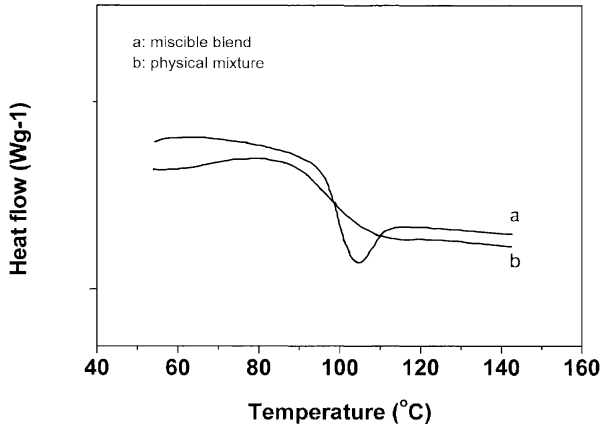

Figure 3.12. Heat flow versus temperature data for (a) the miscible blend and (b) the physical mixture (PMMA/SAN, 50/50 (wt/wt)).

the usefulness of the dC_p/dT signal in studying polymer–polymer miscibility in situations with similar T_gs, miscible and physical blends of SAN and PMMA were designed.

Figures 3.12 and 3.13 show the heat flow and the heat capacity data for the blend and for a physical mixture of PMMA and SAN [39]. From these data, it was not possible to draw any conclusions about miscibility because only one glass transition was observed for both the miscible blend and for the physical mixture. The T_g difference between the two constituent polymers is only about 10°C. However, it is clear from the dC_p/dT versus

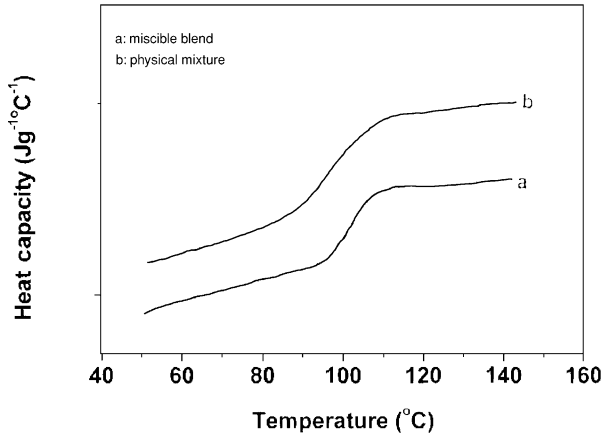

Figure 3.13. Heat capacity versus temperature data for the same (a) miscible blend and (b) physical mixture. The data are shifted vertically for clarity.

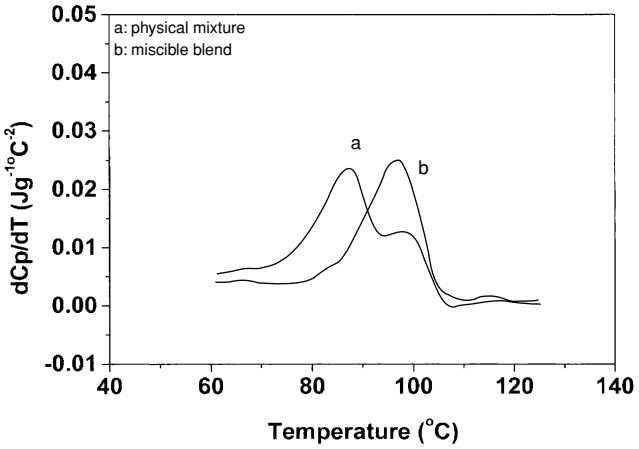

Figure 3.14. Differential of heat capacity versus temperature data for the physical mixture (PMMA/SAN, 50/50 (wt/wt)) and for the blend.

temperature data, shown in Figure 3.14 for both the miscible blend and the physical mixture, that there are differences. The physical mixture shows two clearly resolved transitions which appear to be the result of a simple linear addition of the dC_p/dT signals of the constituent polymers. The miscible blend shows the expected single glass transition.

Figure 3.15 shows the glass transition temperatures plotted versus composition for these PMMA/SAN blends. This shows a positive deviation from linearity often observed for miscible blends and ascribed to specific interactions between segments [6,38].

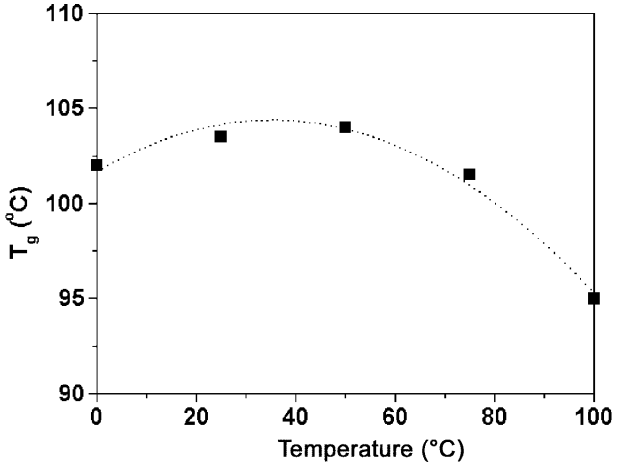

Figure 3.15. Glass transition temperature versus composition for PMMA/SAN (18 wt% AN) miscible blends.

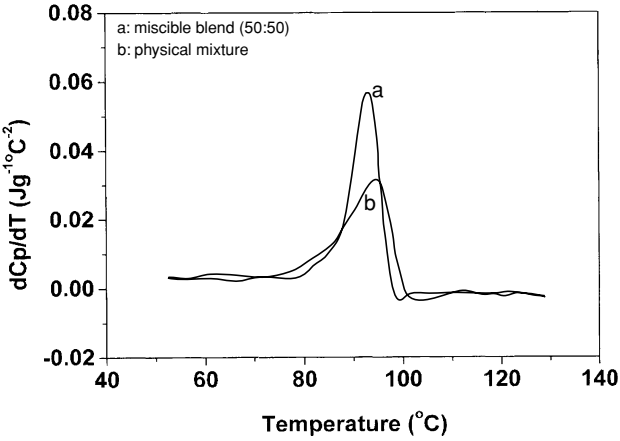

Figure 3.16. Comparison of (a) the miscible blend and (b) the physical mixture (PMMA/SAN, 50/50).

Figures 3.16 and 3.17 show results for a miscible blend and its equivalent physical mixture based on PMMA and a SAN with a 25 wt% AN content. The T_g difference for PMMA and this SAN is approximately 5°C. A single peak in the dC_p/dT signal is very clear for the, by definition, phase separated physical mixture, indicating that it is very difficult to detect miscibility in blends if the difference of T_gs is around this value. However, it is the case that the physical blends show broader transitions than do the miscible ones.

For most polymer pairs to be miscible, an exothermic interaction is required. Nandi *et al.* [40] studied the miscibility of poly(methyl acrylate) (PMA) and poly(vinyl acetate) (PVAc) in several solvents by the inverse

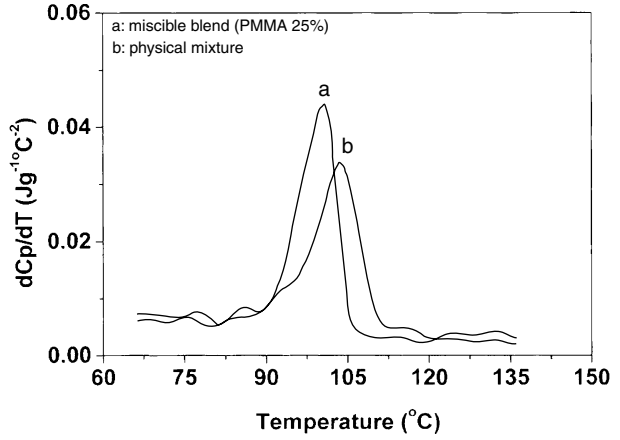

Figure 3.17. Comparison of (a) the miscible blend with (b) the physical mixture (PMMA/SAN, 25/75).

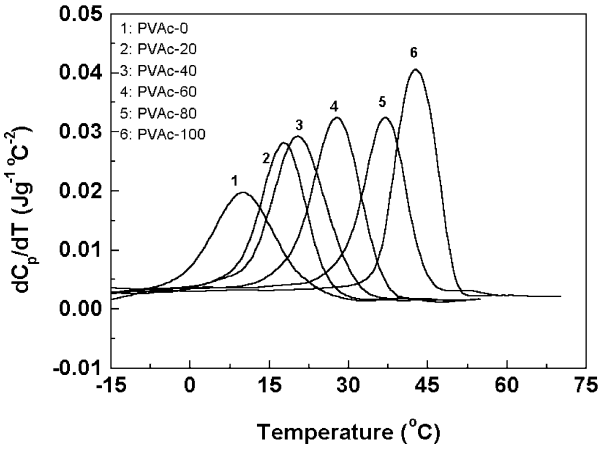

Figure 3.18. dC_p/dT versus temperature data for different PMA/PVAc blend compositions.

gas chromatography method. They concluded that the PMA/PVAc blend is miscible, and that no specific interactions are operative.

Figure 3.18 shows the dC_p/dT signal versus temperature for different PMA/PVAc blend compositions. The dC_p/dT signal showed a high degree of symmetry, which implies that the miscibility level is high. Compare this with the behaviour of PVC/poly(ethyl methacrylate) (PEMA) blends.

Perrin and Prud'homme [41] studied, by means of conventional DSC, the miscibility of PVC blended with PEMA. They showed this system to be miscible. The T_g difference was about 12°C. Using their experimental conditions [41], the miscibility of this blend was studied again by means of MTDSC. Figures 3.19 and 3.20 show, respectively, the changes of heat

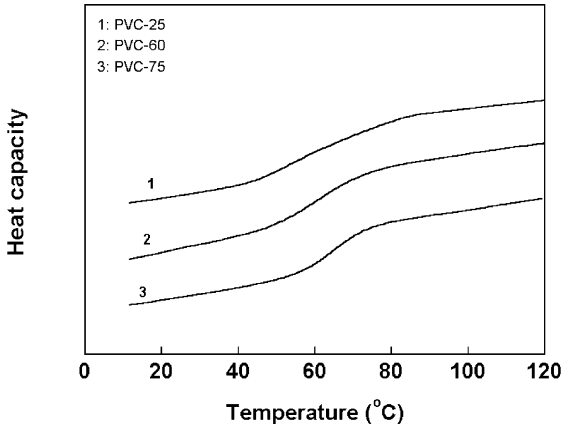

Figure 3.19. Heat capacity versus temperature for PVC/PEMA blends.

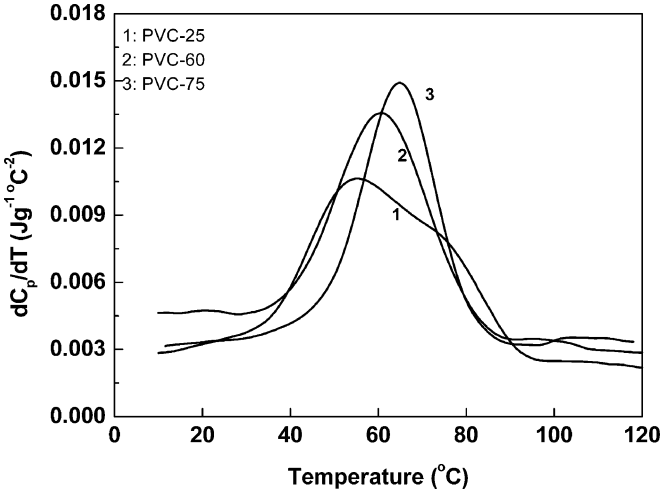

Figure 3.20. dC_p/dT versus temperature for PVC/PEMA blends.

capacity and dC_p/dT versus temperature for the PVC/PEMA blends with 25/75, 60/40 and 75/25 (by weight) compositions. The heat capacity signals show that this blend system may be miscible. However, the dC_p/dT signal for the 25/75 PVC/PEMA blend showed that this blend was not fully miscible. The dC_p/dT signals show that the levels of miscibility of the 60/40 and 75/25 PVC/PEMA blends were higher than that of the 25/75 PVC/PEMA blend. This further emphasises that polymer–polymer miscibility can be checked sensitively using the dC_p/dT signal.

Figures 3.21 and 3.22 show the changes of T_gs and ΔC_p versus composition for some PMA/PVAc blends. The following relations hold for T_g and ΔC_p.

$$T_g = w_1 T_{g1} + w_1 T_{g2} \tag{12}$$

$$\Delta C_p = w_1 \Delta C_{p1} + w_1 \Delta C_{p2} \tag{13}$$

The ΔC_p term is a significant parameter because it appears in the Ehrenfest equation [42]. Perhaps, in polymer blends, the intermolecular contribution to ΔC_p plays a more important role than in many common homopolymers and copolymers.

To date, many supposedly miscible polymer pairs [5,6,13,14,42] have been reported in the literature. However, in some cases [13,14], the breadth of the glass transition region, ΔT_g, taken as the difference between the onset and completion temperatures, is quite broad. For some blend systems, ΔT_g values approach 100°C [13,14]. The transition region may also be

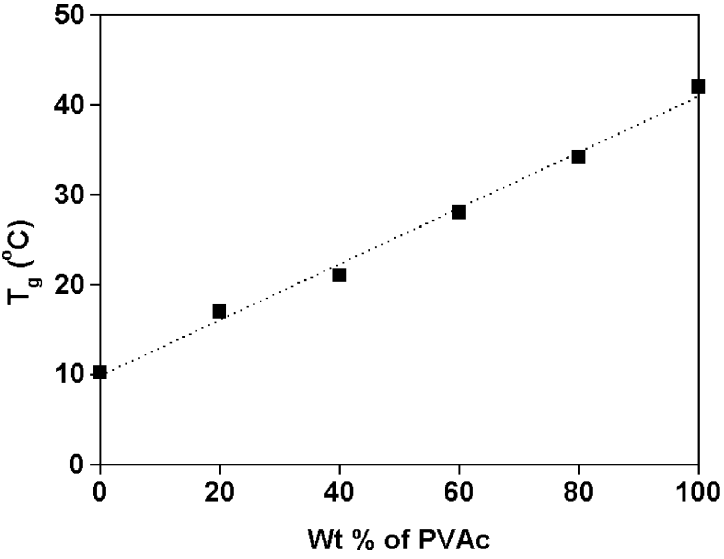

Figure 3.21. Glass transition temperature versus composition for PMA/PVAc blends.

asymmetrical. Because conventional DSC is not sensitive enough and lacks good resolution, overlapping T_gs and interfaces resulting from partial miscibility, cannot be separated. It is possible that some incorrect conclusions have been reached [13,14] for polymer blends that have quite large ΔT_gs [13,14]. To study this problem, the poly(epichlorohydrin) (PECH)/PMMA blend system was chosen for further investigation using MTDSC.

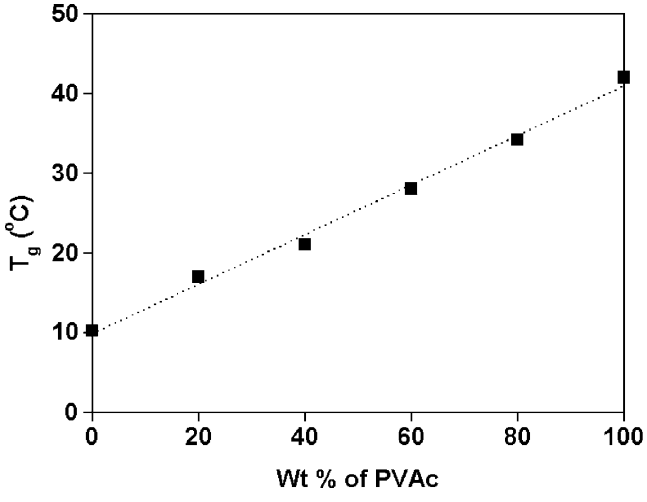

Figure 3.22. Plot of ΔC_p versus composition for PMA/PVAc blends.

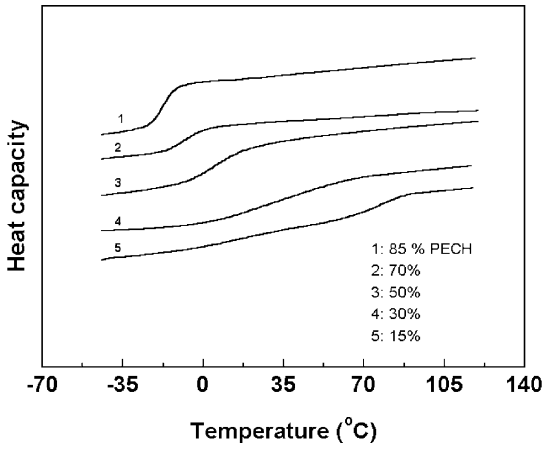

Figure 3.23. Heat capacity (arbitrary scale) versus temperature data for PECH/PMMA blends.

Figure 3.23 shows the change of heat capacity with temperature for five different compositions. These thermograms appear to offer essentially the same interpretation as the results presented by Higgins and co-workers [43] and by Fernandes *et al.* [13,14]. A single and broad T_g transition is seen indicating that the blend is miscible. However, SANS results reported by Higgins and co-workers [43] showed the blend system to possess two phases, indicating that it is essentially immiscible. The dC_p/dT versus temperature data for PECH/PMMA blends at 100/0, 85/15, 70/30, 50/50, 30/70, 15/85 and 0/100 (wt/wt) compositions were checked. The results are shown in Figures 3.24(a)–(g). The dC_p/dT signals give detailed and clear information about miscibility. For pure PECH and PMMA, the transitions are highly symmetrical. For the 85/15 PECH/PMMA blend, the transition peak shows the same behaviour as PECH, or PMMA, in that it is highly symmetrical. This implies that at this composition the polymers are miscible. For the 70/30 PECH/PMMA blend, there is a weak transition between 40 and 100°C. For the 30/70 PECH/PMMA blend, there is obviously phase separation. The dC_p/dT signal shows two transitions. Because the two components have very similar refractive indices [43], it is very difficult to check the phase separation behaviour using optical methods. For the 50/50 blend, the transition peak is markedly asymmetrical, and exhibits a shoulder. At the 15/85 composition, the dC_p/dT signal shows two separated transition peaks clearly confirming immiscibility. Table 3.3 shows the T_g and the ΔT_g values, which were defined as shown in Figure 3.24(g). The correlation lengths shown in Table 3.3 were obtained from the literature [43]. The value for the 15/85 PECH/PMMA blend was omitted because the dC_p/dT signal from this system showed two clear transitions indicating that this correlation length had

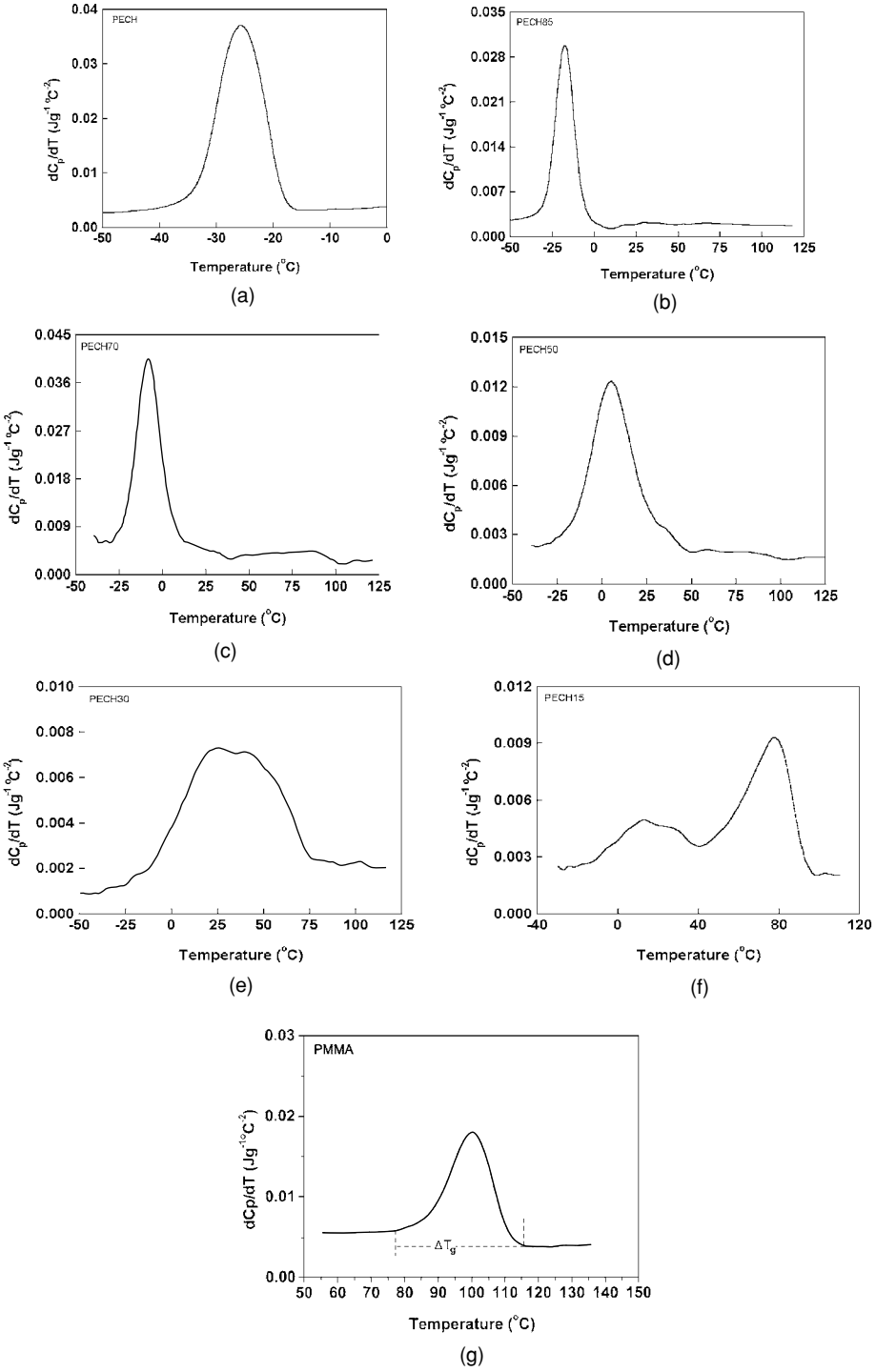

Figure 3.24. (a–f) dC_p/dT versus temperature data for PECH and the PECH/PMMA blends; (g) definition of ΔT_g.

Table 3.3. Glass transition and ΔT_g for the PECH/PMMA blends

PECH/PMMA	T_g (°C)	ΔT_g (°C)	Correlation length (nm) (Ref. [43])
100/0	−26	20	–
85/15	−17	26	–
70/30	–	65	14
50/50	–	80	37
30/70	–	100	47
15/85	Two phase transition signals		
0/100	102	40	–

no physical meaning. It can be seen that the ΔT_g values of the PECH/PMMA blends are quite large and increase with increasing correlation length.

For the PMMA homopolymer, the onset temperature was about 80°C. For PECH, the completion temperature was about −18°C. Obviously, the large ΔT_g values are not due to the fact that the completion of the lower transition and the onset of the higher transition cannot be resolved [43]. The conclusion is that these blend systems exhibit interfaces. The PECH/PMMA blends are, therefore, partially miscible. It is this partial miscibility that causes the large ΔT_g values. It is concluded that most of the PECH forms a mixed phase with PMMA for the 50/50 and 70/30 PECH/PMMA blends. However, for the 30/70 PECH/PMMA blend, there are predominantly PECH-rich and PMMA-rich phases.

For fully miscible systems, the deviation, δT_g, defined as $\delta T_g = \Delta T_g - (w_1 \Delta T_{g1} - w_2 \Delta T_{g2})$, is, by definition, very small. Table 3.4 shows δT_g

Table 3.4. δT_g values for PECH/PMMA, PS/PPO and PMA/PVAc blends

PECH/PMMA	δT_g (°C)
100/0	0
85/15	5
70/30	39
50/50	50
30/70	66
0/100	0
PS/PPO	
100/0	0
75/25	1
50/50	−1
25/75	−1
0/100	0
PMA/PVAc	
100/0	0
75/25	0.5
50/50	1
25/75	−0.5
0/100	0

values for PECH/PMMA, PS/PPO and for PVAc/PMA blends over a range of compositions. Clearly, the immiscible system shows the largest δT_g value.

SANS is able to distinguish between micro-phase separation and concentration fluctuations [43]. However, SANS results showed curves for four blend compositions (PECH/PMMA: 70/30, 50/50, 30/70 and 15/85) which were very similar (Ref. [43]). There was no obvious trend in scattered intensity with composition. These data were fitted by a two function scattering law assuming that the sample was phase separated, but that within the domains, a single-phase scattering law prevailed. Higgins' results [43] showed that it is more probable that the very large concentration fluctuations which gives rise to the Debye–Bueche neutron scattering are also responsible for the extraordinarily broad ΔT_g in this blend. Because the curves for the four blend compositions [43] were very similar, it is difficult to obtain more detailed information about morphology and the concentration distribution in domains from these SANS results. Checking the dC_p/dT signal versus temperature for the four blend compositions, it was found that the four dC_p/dT signals versus temperature were very different, indicating that this approach could prove useful in obtaining a fuller understanding of phase morphology.

For different domains, the concentration distribution will be different. These different domains will show different glass transition behaviour. The system may be divided into many sub-systems, 1, 2, 3, . . . , n each with a corresponding T_g: T_{g1}, T_{g2}, T_{g3}, . . . , T_{gn}. When the difference in concentration between domains is small, the glass transition may be considered to arise from a continuous distribution of such sub-systems.

From the above discussion, it is concluded that the dC_p/dT signal from MTDSC can give very useful information about polymer–polymer miscibility more directly than can the scattered intensity signal from SANS experiments.

4.2 INTERFACE DEVELOPMENT BETWEEN COMPATIBLE POLYMER FILMS

The interface between two polymers, whether compatible or incompatible, is a region of finite thickness within which the composition varies continuously from one bulk phase to the other [44]. This interfacial region is formed by interdiffusion of the two continuous phases, driven by the chemical potential gradient. In an incompatible system, the equilibrium interfacial thickness is attained when the entropy effect equals the enthalpy effect [45–48], giving a thickness of typically 1–20 nm, depending

on the degree of compatibility [45–49]. The formation of a diffuse interface is important in adhesion [45–48,50,51], phase separation and the consequent morphology in polymer blends [52–54], welding and crack healing [55,56], and co-extrusion [57]. In these applications, the final properties are determined by the thickness of the interface and the concentration profile of the two polymers across that interface. Interdiffusion at polymer–polymer interfaces is a strong function of temperature, mutual compatibility, molecular weight, molecular weight distribution, chain orientation and the molecular structure of the polymers concerned [58–62]. For example, Brochard-Wyart and de Gennes [62,63] showed that under asymmetrical conditions polymers reptate in a set of moving tubes. Brochard-Wyart and co-workers [64,65] showed that the initial asymmetry in the kinetics induced by the chain end segregation is healed after a characteristic Rouse time. Jabbari and Peppas [66] showed experimentally that for polymer pairs with dissimilar physical properties the concentration profile is highly asymmetric.

To describe the effect of the above parameters on interdiffusion, de Gennes [67] used the chemical potential gradient as the driving force for interdiffusion. Assuming that the fluxes of the two components were equal, but opposite, Brochard-Wyart *et al.* [68] derived the slow-mode theory for interdiffusion at polymer interfaces.

$$D = \Lambda_A \Lambda_B / (\Lambda_A + \Lambda_B)[1/(N_A \phi_A) + 1/(N_B \phi_B) + 2\chi] \tag{14}$$

D is the interdiffusion coefficient, Λ_A and Λ_B are the segment mobilities of polymers A and B, respectively, N_A and N_B are the number of repeat units in each polymer, ϕ_A and ϕ_B are the molar fractions of each polymer and χ is the Flory–Huggins interaction parameter. The slow-mode theory predicts that interdiffusion is dominated by the slow-diffusing polymer. Later, de Gennes [69] showed that the mobility was directly related to the diffusion coefficient of each polymer. The limitation of this theory is that it assumes that the fluxes of the two polymers are equal and opposite, which means that the interface remains symmetrical as interdiffusion proceeds.

On the other hand, Kramer and co-workers [70,71] showed that, for polymer pairs with different molecular weights, the interface moves towards the polymer with the lower molecular weight as interdiffusion proceeds. Kramer *et al.* [72] and Sillescu [73] described interdiffusion in systems with a moving interface by unequal fluxes of polymers A and B, which were balanced by a net flux of vacancies across the interface. By assuming that the chemical potential of these vacancies was zero in the melt state, but the flux of vacancies was finite, they derived the following equation for the

interdiffusion coefficient.

$$D = \phi_A\phi_B/(\phi_B/\phi_A\Lambda_A + \phi_A/\phi\Lambda_B)[1/(N_A\phi_A) + 1/(N_B\phi_B) + 2\chi] \quad (15)$$

In the fast-mode theory, the overall mobility is linearly related to the mobility of each component, indicating that the interdiffusion coefficient is dominated by the faster-moving component.

Akcasu *et al.* [74] attempted to identify the fast and slow modes with the two modes observed in dynamic scattering experiments from ternary polymer solutions. They defined the vacancies as the third component in a mixture of A and B polymers and concluded that the slow mode was obtained when vacancies were gradually removed, resulting in an incompressible binary mixture of A and B. The fast mode was obtained in the opposite limit of high vacancy concentration or a matrix with very high mobility. Since the polymer mobility and the vacancy concentration are small below, and high above, T_g, this suggested that the slow and fast-mode theories described interdiffusion below and above T_g, respectively.

In fact, most of the interdiffusion data in the literature [69–72,75,76] that were collected above T_g, are consistent with the fast-mode theory of interdiffusion. Kramer *et al.* [72] used Rutherford back-scattering spectroscopy to follow the movement of a gold marker at the interface between PS and deuterated PS (d-PS) with different molecular weights. They observed movement of the interface towards the fast-diffusing component. Reiter *et al.* [77] used X-ray reflection spectrometry also to follow the movement of a gold marker placed at the interface between PS and d-PS. They were able to detect a delay in the onset of interface movement, which depended on molecular weight, and there was a strong indication of a correlation between this induction time and the reptation time of the chain. Wu *et al.* [78] investigated the structure and kinetics of the diffuse interface between PMMA and poly(vinylidene fluoride) in the melt. They too detected interface movement using a gold marker. The structure and kinetics confirmed the predictions of the reptation theory [55]. The interfacial thickness was seen to grow with $t^{1/2}$, where t is the diffusion time.

Interdiffusion between two compatible polymers has also been studied by means of X-ray reflection spectrometry [77], TEM [78], Rutherford backscattering spectrometry [72] and forward recoil spectrometry [79]. We will now report on the use MTDSC to study symmetrical and asymmetrical interdiffusion between two compatible polymers. The main aim is to provide a relatively accessible method to investigate symmetrical and asymmetrical interdiffusion. Conclusions on whether symmetrical or asymmetrical interdiffusion occurs between two compatible polymers have been based on

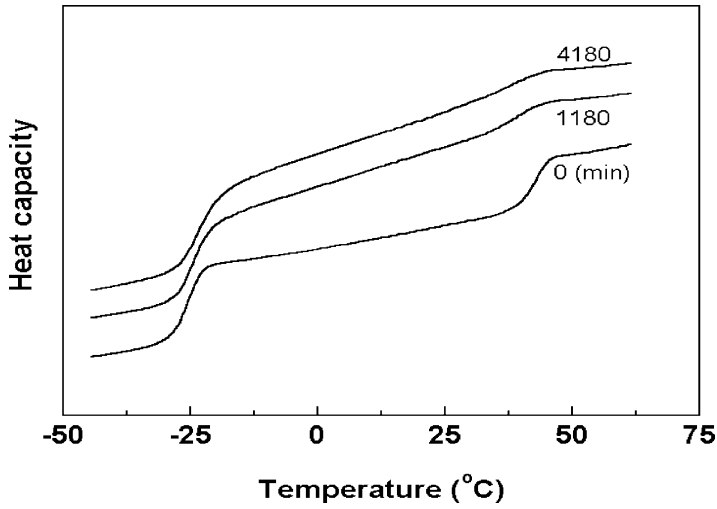

Figure 3.25. Heat capacity (arbitrary units) versus temperature at different diffusion times for the PECH–PVAc combination.

the diffusion coefficients of the two polymers and on measurements of the diffusion profile [78,79].

4.2.1 Asymmetrical Interdiffusion: Polyepichlorohydrin/Poly(vinyl acetate)

Figure 3.25 shows the changes of heat capacity with temperature for the polyepichlorohydrin (PECH)/poly(vinyl acetate) (PVAc) combination at different diffusion times. In the glass transition region, the heat capacity traces are different for the different diffusion times.However, it is difficult to draw out more detailed information from these traces. The dC_p/dT curves, however, clearly showed that an interface is formed by thermal diffusion. (see Figure 3.26). This is shown by the increase in the dC_p/dT signal between the two glass transitions. With increasing diffusion time, the concentration of the interface will change and its thickness will increase.

When a system exhibits an interface, the following equations hold.

$$\Delta C_p = \Delta C_{p^1} + \Delta C_{p^2} + \Delta C_{p^i} \tag{16a}$$

$$\Delta C_{p^1} = \omega_1 \Delta C_{p^{10}} \tag{16b}$$

$$\Delta C_{p^2} = \omega_1 \Delta C_{p^{20}} \tag{16c}$$

ω_1 and ω_2 are the weight fractions of components 1 and 2, respectively, in the mixed phases. ΔC_{p^i} is the increment of heat capacity of the diffuse interface in its glass transition region, and δ_1 and δ_2 in the following equations are

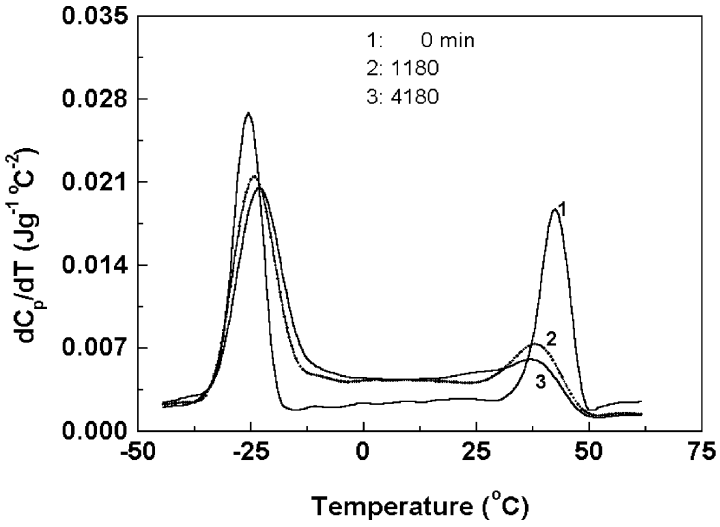

Figure 3.26. dC_p/dT versus temperature at different diffusion times for the PECH–PVAc combination.

the weight fractions in the diffuse interface for polymer 1 and polymer 2, respectively, which can be obtained from these equations.

$$\delta_1 = \omega_{10} - \Delta C_{p^1}/\Delta C_{p^{10}} \tag{17a}$$

$$\delta_2 = \omega_{20} - \Delta C_{p^2}/\Delta C_{p^{20}} \tag{17b}$$

ω_{i0} and ΔC_{pi0} are the weight fraction and the increment of heat capacity of the polymers before mixing.

Using Eqs. (16) and (17), the weight fraction of interface can be calculated.

Figure 3.27 shows the change of weight fraction of the interface with time and Figure 3.28 shows the changes of weight fraction, ω_A and ω_B, of the PECH and PVAc components in the interface with time. Clearly, the change of ω_A and of ω_B with time are different. This indicates that the diffusion rate for PVAc is faster than that for PECH. The interdiffusion for this polymer pair is, thus, asymmetrical.

Now, consider the average value, ρ, of the density of PECH and PVAc in the diffuse interface. Assuming ρ approximates to the linear sum of ρ_A and ρ_B,

$$\rho = (\rho_A \omega_A W_{PECH} + \rho_B \omega_B W)/(\omega_A W_{PECH} + \omega_B W_{PVAC}) \tag{18}$$

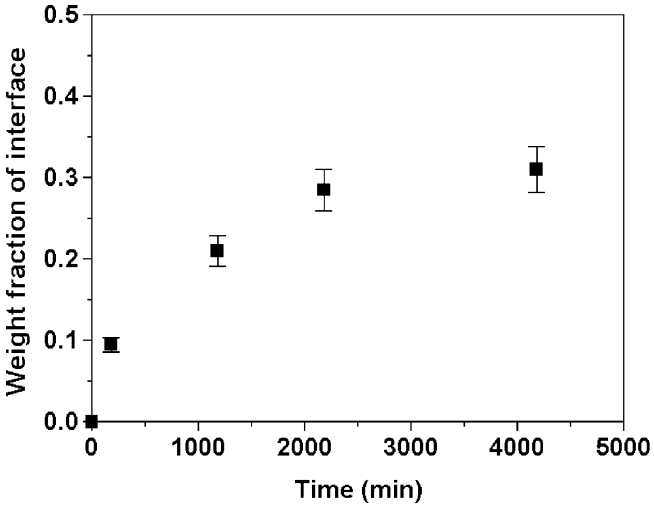

Figure 3.27. Weight fraction of the interface versus diffusion time for the PECH–PVAc combination.

W_{PECH} and W_{PVAC} are the weights of PECH and PVAc, respectively, in the pure phases before mixing. The volume of the interface, V, is given as follows.

$$V = W/\rho \tag{19}$$

W is the mass of the polymers in the interface.

$$W = \phi(W_{\mathrm{PECH}} + W_{\mathrm{PVAC}}) \tag{20}$$

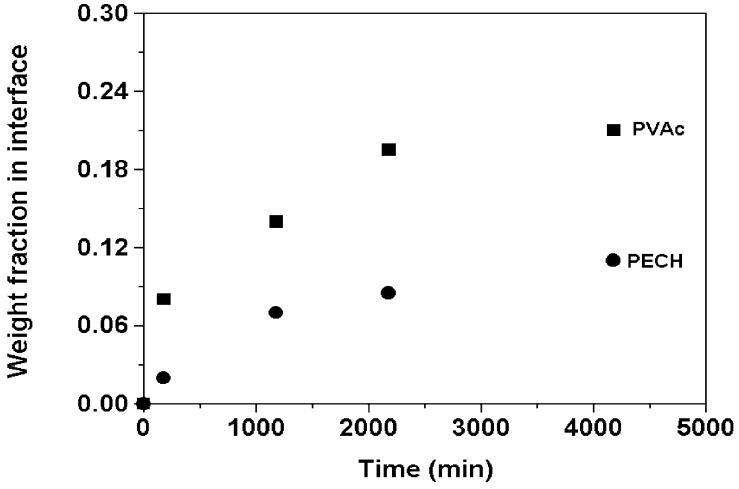

Figure 3.28. Weight fraction of the PECH and PVAc in the interface versus diffusion time.

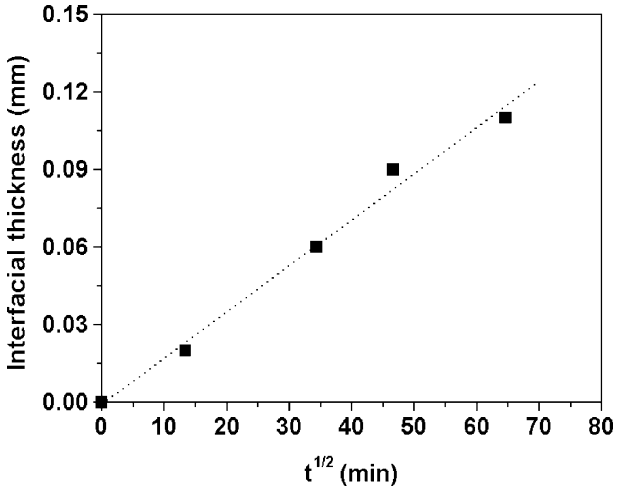

Figure 3.29. Thickness of the interface versus diffusion time for the PECH–PVAc combination.

ϕ is the weight fraction of interface. The average thickness of the interface, d, can be obtained as shown in Eq. (21).

$$d = \phi(W_{\text{PECH}} + W_{\text{PVAC}})/(S\rho) \tag{21}$$

S is the area of the sample, and, therefore, also of the diffuse interface, when considering two superimposed films. The change of thickness of the interface with diffusion time is shown in Figure 3.29. Here, the densities of PECH and PVAc at room temperature were used to calculate the average density, ρ. Obviously, the thickness of interface is a function of diffusion time, t. The interfacial thickness grows according to the following rule which is consistent with the reptation analysis [80] of Wool and Kim [55], Prager and Tirrell [81], Adolf and co-workers [82,83] and Wu *et al.* [78].

$$d \propto t^{1/2} \tag{22}$$

Here, we only give an estimate of the interdiffusion coefficient of the PECH/PVAc pair at 100°C. Based on Fick's diffusion theory [84], the mean-square interfacial thickness, r_{eff}, is given by Eq. (23).

$$r_{\text{eff}} = (d)^2 = (2Dt)^{1/2} \tag{23}$$

From Figure 3.30, which shows the change of r_{eff} with time, it can be calculated that D is approximately 6.25×10^{-11} cm^2/s.

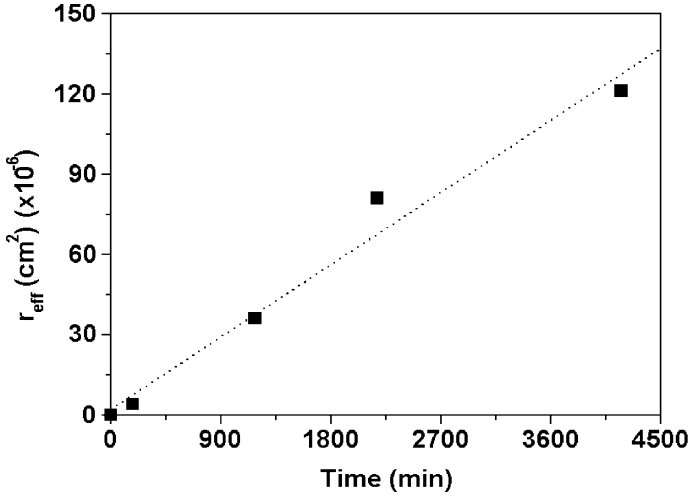

Figure 3.30. Mean-square interfacial thickness versus diffusion time for the PECH–PVAc combination.

4.2.2 *Symmetrical Interdiffusion: Poly(methyl acrylate)/ Poly(vinyl acetate)*

The PMA–PVAc blends are miscible, but show no specific interactions. The interdiffusion coefficient will be as follows.

$$D = D_A = D_B \tag{24}$$

Figure 3.31 shows dC_p/dT versus time at 100°C for the PMA/PVAc combination. The dC_p/dT signal shows clearly that an interface is formed by thermal diffusion. This is shown by the increase in the dC_p/dT signal between the two glass transitions. It can also be seen that the PMA, PVAc and interface signals overlap. A peak-resolution technique, with the condition that ΔC_p (observed) = ΔC_p (calculated), can be used to deal with this problem. Figure 3.32 shows the result for the sample annealed for 130 h.

Figure 3.33 shows how the weight fraction of the interface increases with time, whilst Figure 3.34 shows how ω_A and ω_B, the weight fractions of PMA and PVAc, respectively, in the interface change with time. The changes of ω_A and ω_B with time are similar, which indicates that interdiffusion in this particular polymer pair is symmetrical. The change of thickness of the interface with diffusion time is shown in Figure 3.35. Here, the room temperature densities of PMA and PVAc were used to calculate the average density, ρ. Thus, for both symmetrical and asymmetrical interfaces, the growth of interfacial thickness can be described by Eq. (22).

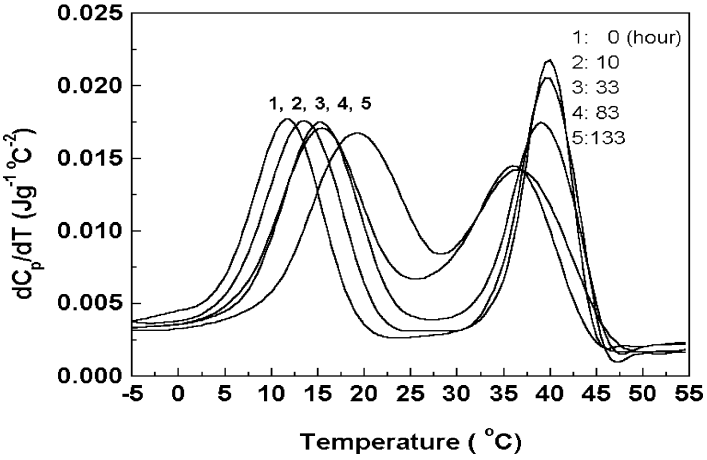

Figure 3.31. dC_p/dT versus temperature data at different diffusion times for the PMA–PVAc combination.

For symmetrical diffusion, the diffusion equation can be solved analytically [84] to give the following solution.

$$\Pi_A(x,t) = 1/2\{1 - \mathrm{erf}[x/(2(Dt)^{1/2})]\} \tag{25a}$$

$$\Pi_B(x,t) = 1/2\{1 + \mathrm{erf}[x/(2(Dt)^{1/2})]\} \tag{25b}$$

Figure 3.36 shows how r_{eff} changes with time. The calculated D value is approximately 4.1×10^{-11} $\mathrm{cm^2 s^{-1}}$.

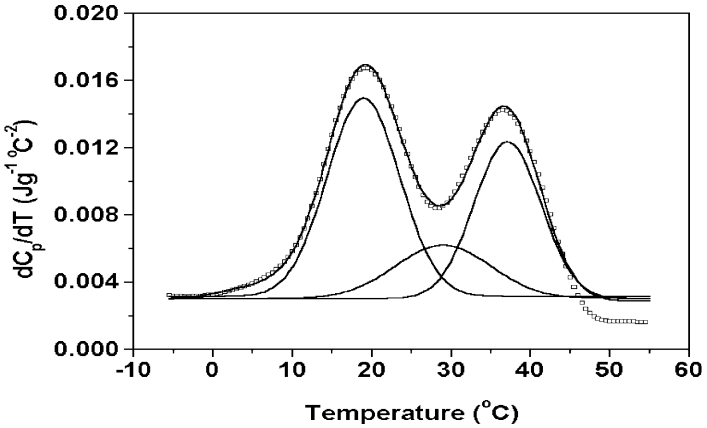

Figure 3.32. Comparison of the multi-peak resolution results with the experimental data (□) for the PMA–PVAc combination annealed at 100°C for 130 h.

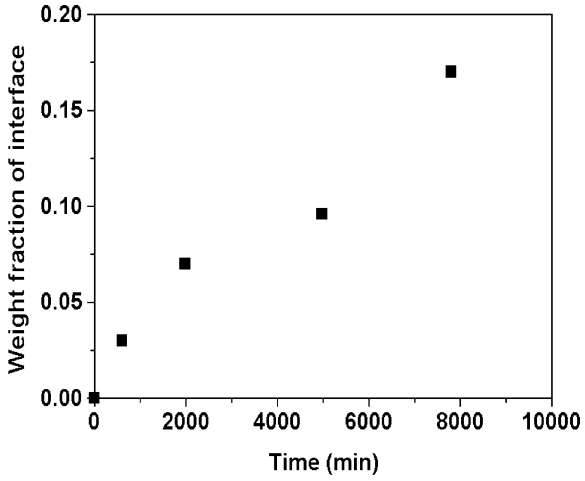

Figure 3.33. Weight fraction of the interface versus diffusion time for the PMA–PVAc combination.

From the above discussion, the symmetrical and asymmetrical interdiffusion between two compatible polymers can be followed based on measurements of the component weight fractions in the interface region.

$\omega_A = \omega_B$ symmetrical interdiffusion

$\omega_A \neq \omega_B$ asymmetrical interdiffusion

The difficulty in a full test of Eqs. (14) and (15) lies in the considerable amount of data required. Tracer diffusion coefficients [72], which are related

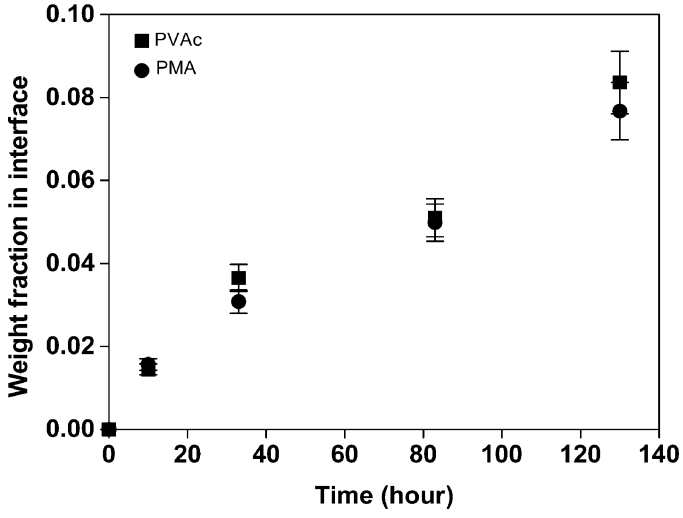

Figure 3.34. Weight fraction of the PMA and PVAc in the interface versus diffusion time.

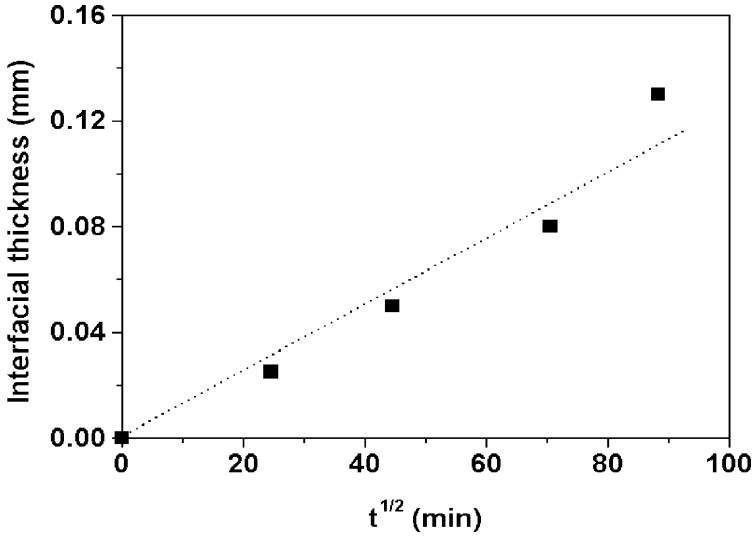

Figure 3.35. Thickness of the interface versus diffusion time for the PMA–PVAc combination.

to Λ_A and Λ_B as a function of composition, as well as the Flory interaction parameter, will, in general, be needed to predict D. These quantities are not easy to measure, so that experimental data are quite scarce.

Equation (14) always predicts a lower value of D than does Eq. (15). In a system where one of the tracer diffusion coefficients is very small, Eq. (14) predicts that D, will also be small, leading to the notion that interdiffusion

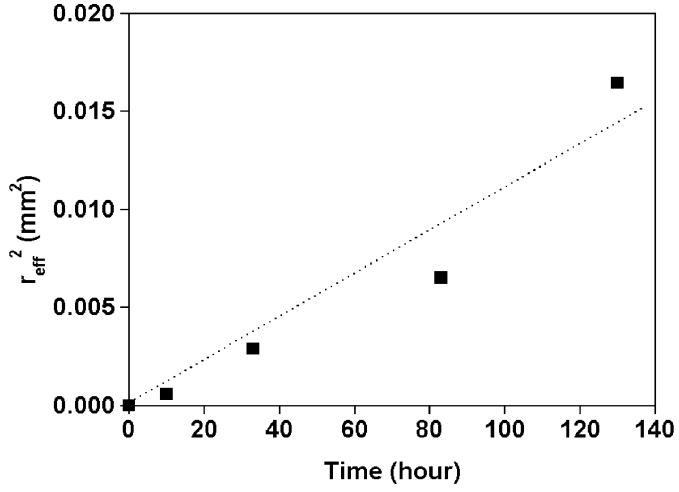

Figure 3.36. Mean-square interfacial thickness versus diffusion time for the PMA–PVAc combination.

is "controlled" by the less mobile species. Equation (15) makes the opposite prediction. Murschall *et al.* [85] have investigated the temperature dependence of D using light scattering and found that the parameters describing interdiffusion as a function of temperature are very close to those describing self-diffusion of the less-mobile species. They concluded that this fact implies that Eq. (14) accurately describes interdiffusion in polymer–polymer systems.

On the other hand, results from recent experiments where the displacement of markers across a polymer–polymer interface has been observed [75,81] have been interpreted to favour Eq. (15). This conclusion has been based largely on arguments concerning the compressibility of the system. Equation (14) implies an incompressible system, whereas Eq. (15) implies a compressible one.

A better approach is to measure the molecular weight dependence of D in entangled polymer mixtures as was done by Gilmore *et al.* [86]. These authors found that, at constant N_A, the dependence of D on N_B could be represented by Eq. (26).

$$D = \alpha + \beta / N_B \tag{26}$$

Assuming a reptation-type behaviour for D_A and D_B, this result is in good agreement with Eq. (15), where α and β will be functions of composition. Equation (14) is not consistent with Eq. (26).

Figure 3.37 shows the changes of the weight fraction of PVAc and PECH in the interface with $t^{1/2}$.

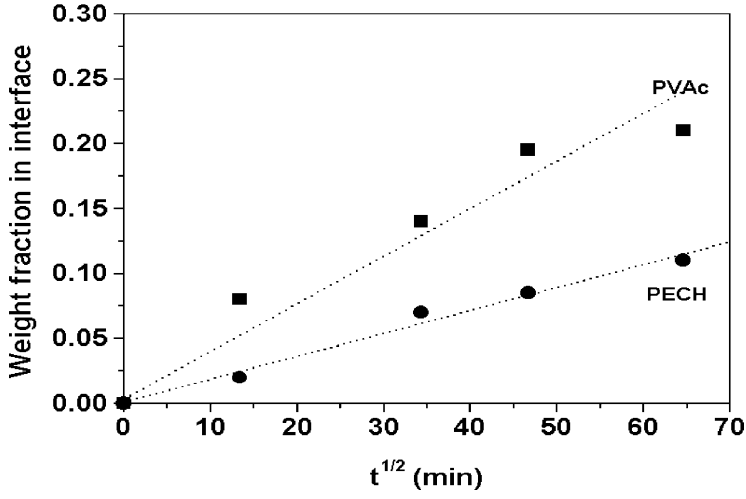

Figure 3.37. Weight fraction of PECH and PVAc in the interface versus diffusion time. (Dashed line is the best fit to the experimental data).

Because d_{PECH} (diffusion thickness) is proportional to ω_{PECH} (in the interface) and because D_{PECH} (or D_A) is proportional to d_{PECH} (diffusion thickness) and, in addition, because d_{PVAC} (diffusion thickness) is proportional to ω_{PVAC} (in interface) and because D_{PVAC} (or D_B) is proportional to d_{PVAC} (diffusion thickness) the reptation behaviour for D_A and D_B is confirmed experimentally. This is evidence in support of Eq. (15).

4.3 STRUCTURED LATEX FILMS

Over the past several years, concern for the environment has generated many instances where there is a need to turn from a polluting technology to one that is more benign. Since these changes are driven by factors outside the technology, this can have the result that the new system has poorer performance characteristics than the technology being replaced. Under these circumstances, it becomes important to understand the origins of good performance, so that adequate, or even improved, performance can be achieved with a new technology that is safer to the environment.

One current example of this situation is the impact on coatings technology of the stricter regulations on volatile organic compound emissions. Because of these restrictions, the use of waterborne latex-based coatings is expanding into areas such as automotive and industrial coatings, traditionally reserved for organic solvent-based systems. The industrial and automotive markets have resisted this change because the waterborne latex coatings are as yet unable to achieve the same high level of performance as the traditional solvent-based systems [87].

In solvent-based coatings, the polymer molecules are entangled and fully interpenetrating as they are applied to a surface. Solvent evaporation leaves a uniform film of low permeability. In latex coatings, the polymers are in the form of discrete (latex) particles that must coalesce during drying and subsequent ageing to form a protective film. Such films are more permeable, especially to moisture, than the corresponding solvent-based films [88] and they provide somewhat poorer protection of the underlying substrate. There are many reasons for the differences in properties between the two types of coating, but it is clear that the "quality of coalescence" of latex coatings has an important effect on the final film properties. This process of coalescence is one of the most important aspects of latex film formation. An understanding of the mechanism by which coalescence occurs is crucial for further advances in this area.

Film formation from polymer latexes is a complicated, multi-stage phenomenon and has been the subject of much theoretical and experimental attention. Many studies of the individual stages, utilising a variety of different techniques, have been published. The use of latex films to investigate

molecular interdiffusion is important in terms of theory development in situations such as coatings coalescence, welding and crack healing. There are two basic methods of studying the diffusion of polymer molecules across the boundary between particles in a latex system: SANS [89] and fluorescence techniques [90]. The advantages of SANS lie in its high sensitivity and its ability to determine, easily, the diffusion coefficient and the chain interpenetration depth [89].

The other interesting method utilises fluorescence measurements. This approach has been mainly applied to latex film formation by Winnik and Wang [90]. In this technique, latex is prepared in two different batches. In one batch, the chains contain a "donor" group, while in the other, an "acceptor" group is attached. The interdiffusion of polymer chains between neighbouring latex particles is then studied by direct non-radiative energy transfer measurements.

AFM and TEM techniques can also give information about the change of particle size during coalescence. Goh *et al*. [91] and Hourston and coworkers [92] have studied the integration of a latex film using AFM. They calculated the surface diffusion coefficient based on the classical diffusion model and found it to be 1×10^{-13} cm^2 s^{-1}, which is three to four orders of magnitude larger than that obtained by SANS [89] (10^{-16} to 10^{-17} cm^2 s^{-1}). The difference was attributed to the extra driving force from the surface free energy, which causes faster diffusion near the surface than is the case in the bulk.

Molecular interdiffusion in a core (poly(butyl methacrylate)–shell (poly(butyl methacrylate-*co*-butyl acrylate) latex, which exhibits miscibility between the core and shell polymers, has been studied [93]. The volume fraction of mixing and the inter-particle penetration distance increased with annealing time [93]. In other core–shell latex films, phase separation can occur upon annealing, because of immiscibility of the core and shell phases.

As has already been made clear, interdiffusion is of great importance for the development of the physical properties of latex films [94]. In order to learn how to optimise the performance of a wide variety of coatings formulations, a deeper understanding of the coalescence process is needed. The essential feature that one needs to understand is the role of inter-particle polymer diffusion once the water has evaporated and the nascent film has formed. Although, as reported above, latex film coalescence processes have been studied [90–94], a much better understanding of these processes is needed. In this section, the process of core–shell latex film coalescence and the dynamics of surface structure development of latex films will be discussed in the light of recent MTDSC studies by the authors.

It has already been shown above that the dC_p/dT signal readily provides fruitful information about multi-phase polymer materials. Measurement of the ΔC_p values of the pure shell and core phases at their T_gs leads to

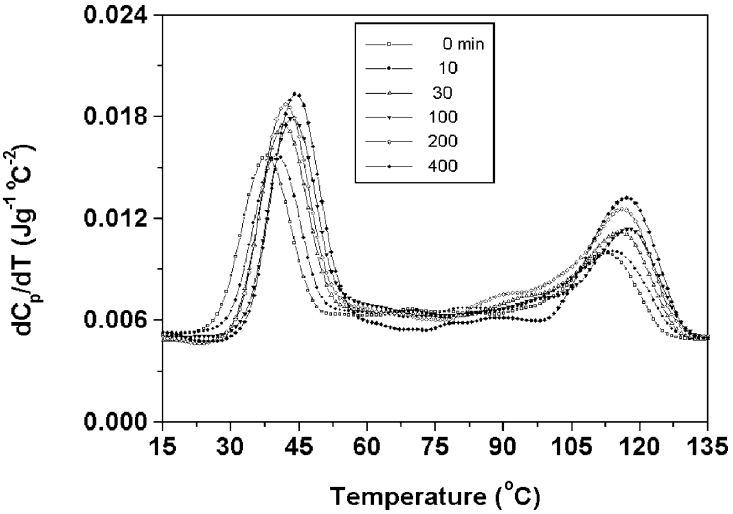

Figure 3.38. dC_p/dT versus temperature data for a PMMA/PVAc latex film annealed at 140°C for different times.

information about the interface between these regions. For core–shell latex particles, interfacial thickness and the weight fraction of that interface are two important property-influencing parameters. However, it is difficult to estimate these parameters for core–shell latexes from TEM and DMTA experiments. However, based on MTDSC measurements, these parameters can be obtained.

Figure 3.38 shows the dC_p/dT versus temperature signals for a PMMA/PVAc core–shell (50/50) latex film after different annealing times at 140°C and Figure 3.39 shows the same signal for the PMMA phase when annealed at 150°C for different times [95]. With increasing time, the dC_p/dT signal obviously changes. The magnitudes of the dC_p/dT signals for the pure PMMA and PVAc components increase, i.e. the ΔC_p values increase indicating that the weight fractions of the pure PMMA and PVAc components increase. The densities of PMMA and PVAc are about 1.19 and 1.192 g cm^{-3} [96], respectively. For an ideal PMMA/PVAc core–shell latex particle, the following relationship holds between the radius, R, of the core and the thickness, ΔR, of the shell.

$$3R^2\Delta R + 3R\Delta R^2 + \Delta R^3 = R^2 \tag{27}$$

For the films cast from the PMMA/PVAc core–shell latex, $R + \Delta R$ was found to be 100 nm. Then, R is 79 and ΔR is 21 nm.

Based on MTDSC measurements, the amount of interface in the unannealed PMMA/PVAc core–shell latex was about 44 wt%, a quite large value.

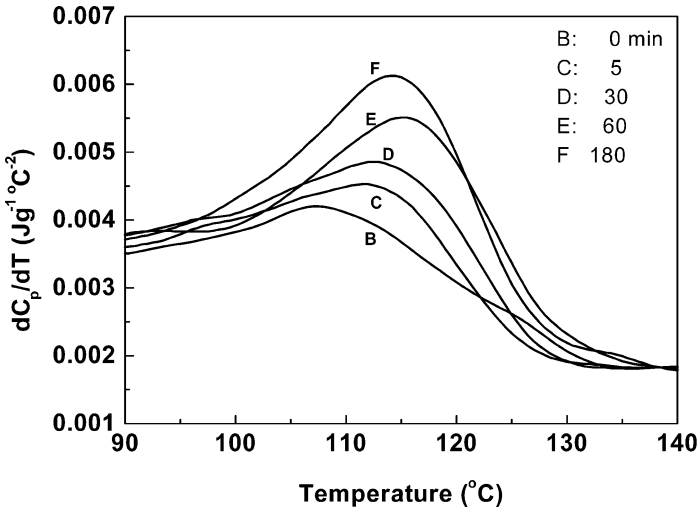

Figure 3.39. dC_p/dT versus temperature data for the PMMA phase in a PMMA/PVAc latex film annealed at 150°C for different times.

This is not surprising because the system is at least partially miscible [35]. When an interfacial phase exists, the shell phase will become thinner and the radius of the core phase will also decrease. For this latex, the interfacial region has a thickness of about 27 nm. This is taking zero annealing time as being a true reflection of the morphology in the original latex particle state. With increasing annealing time, the interfacial thickness decreases. Figure 3.40 shows the change of weight fraction of the interface with annealing time at 150°C. With increasing annealing time, the weight fraction of the

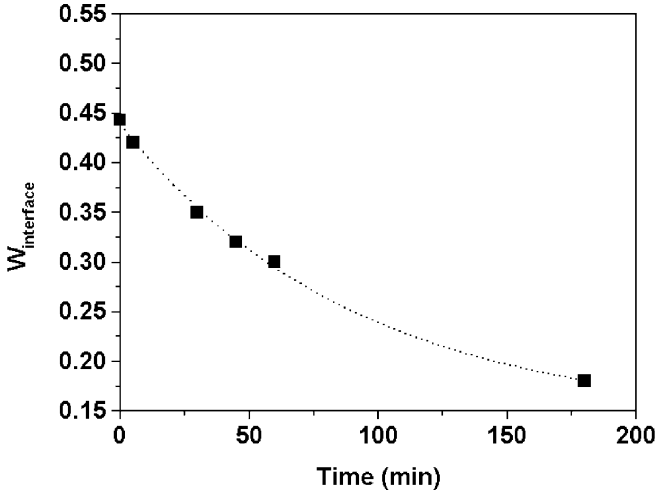

Figure 3.40. Weight fraction of interface versus annealing time at 150°*C* for the PMMA/PVAc core–shell latex.

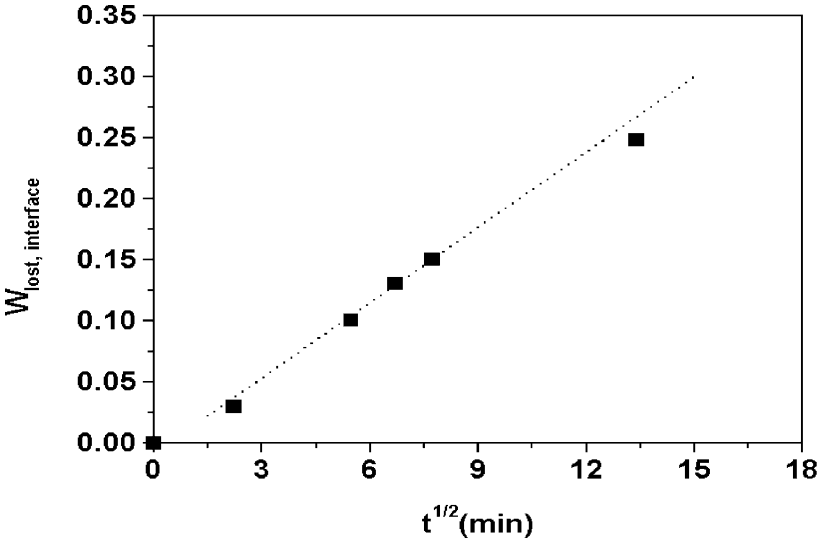

Figure 3.41. Lost weight fraction of the interface versus square root of time.

interface decreases. Figures 3.41 and 3.42 show the changes in the weight fraction, ω_{lost}, of interface for the total and individual parts, respectively [95]. The change with time can be described by Eq. (28).

It is, therefore, confirmed that the macromolecular diffusion during phase separation can be described by the reptation model, i.e. the mechanism of

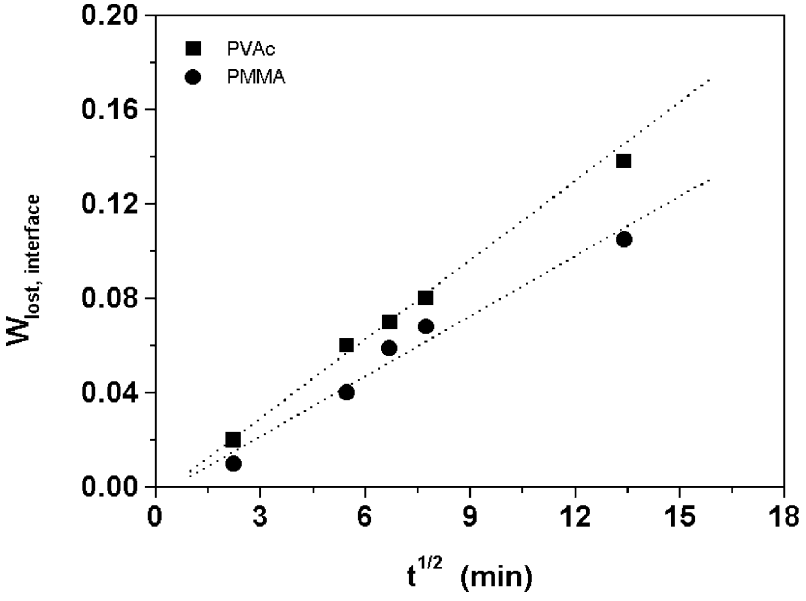

Figure 3.42. Lost weight fraction of the individual components in the interface versus square root of time.

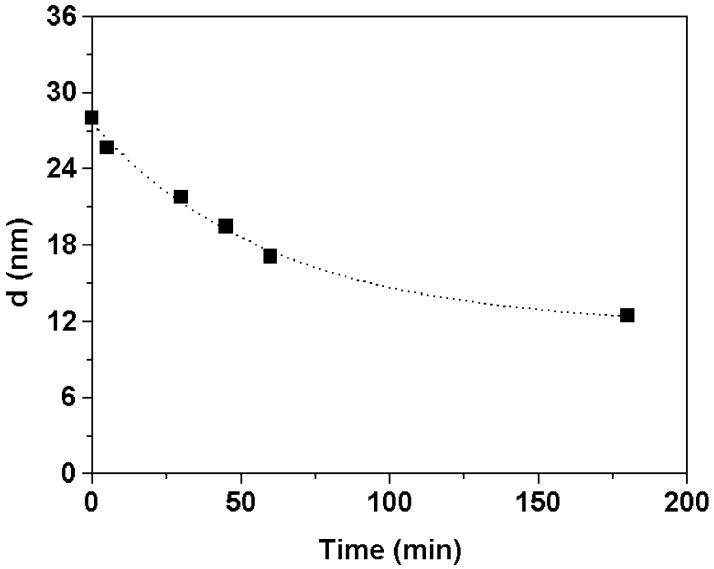

Figure 3.43. Interfacial thickness of the PMMA/PVAc core–shell latex versus time of annealing at 150°C.

phase separation is the same as that in the interdiffusion, discussed previously, of two compatible polymer films.

Figure 3.43 shows the change of interfacial thickness of the PMMA/PVAc core–shell latexes with time [95].

Macromolecular diffusion in the interface between the core and shell phases can be illustrated by a model composed of three parts: core, A, the interface between the core and the shell, AB and the shell phase, B as shown in Figure 3.44. It is assumed here that the core phase is totally covered by the shell phase. The PMMA/PVAc latex is phase-separated at high temperature [97]. During phase separation of the interfacial phase, polymer A in the core does not diffuse out and polymer B in the shell does not diffuse into the AB and core phases. The parameters $C(r, t)$ and $\omega(r, t)$ are the concentrations of polymer A and polymer B which diffuse into the core and shell phases, respectively.

According to Fick's second law,

$$\nabla(DC) = \partial C/\partial t \tag{28}$$

$$D_{\mathrm{A}}[\partial^2 C/\partial r^2 + 2/r\ \partial C/\partial r) = \partial C/\partial t \tag{29}$$

$$D_{\mathrm{B}}[\partial^2 \omega/\partial r^2 + 2/r\ \partial \omega/\partial r) = \partial \omega/\partial t \tag{30}$$

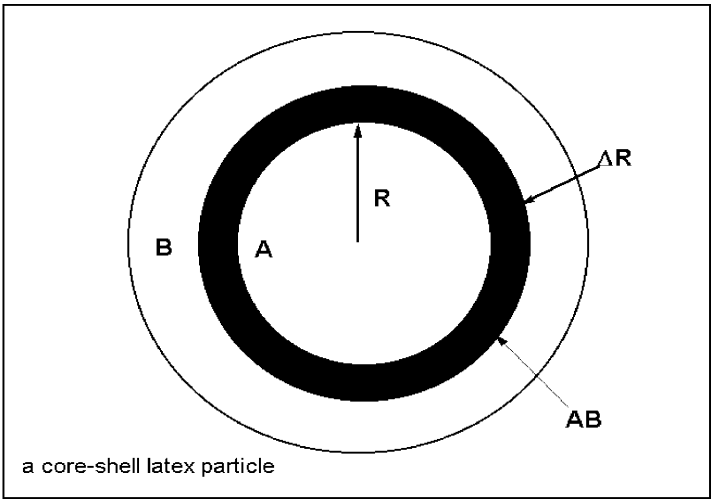

Figure 3.44. Model of a core–shell latex particle with an interphase.

The initial conditions are

$$C(r, 0) = 0 \tag{31}$$

$$\omega(r, 0) = 0 \tag{32}$$

D_A and D_B are the diffusion coefficients of polymers A and B, respectively.

Let $C = rY$, then

$$D_A \partial^2 Y/\partial r^2 = \partial Y/\partial t \tag{33}$$

$$Y(r, 0) = 0 \tag{34}$$

And let $\omega = rZ$

$$D_B \partial^2 Z/\partial r^2 = \partial Z/\partial t \tag{35}$$

$$Z(r, 0) = 0 \tag{36}$$

Taking the Laplace transforms of Eqs. (33) and (35) yields Eqs. (37) and (38).

$$D_A \mathrm{d}^2 Y(r, p)/\mathrm{d}r^2 = pY(r, p) \tag{37}$$

$$D_B \mathrm{d}^2 Z(r, p)/\mathrm{d}r^2 = pZ(r, p) \tag{38}$$

Let

$$F(t) = \int_0^R 4\pi r^2 \, C(r, t)\mathrm{d}r \tag{39}$$

and

$$\Phi(t) = \int_R^{R+\Delta R} 4\pi r^2 \omega(r, t)\mathrm{d}r \tag{40}$$

$F(t)$ and $\Phi(t)$ are the weight fractions of polymer A and polymer B which have diffused into core and shell phases, respectively, at time t. Taking Laplace transforms [95],

$$F(t) = A_o\{R/(\pi D_A t)^{1/2}\exp[-R^2/(4D_A t)] - \mathrm{erf}(R/(4D_A t)^{1/2}) + 1\} \tag{41}$$

A_o is a constant. Equation (41) can be used to simulate the process of phase separation of the interfacial phase and to estimate the diffusion coefficients.

Figure 3.45 compares the calculated and experimental results. $D_A \approx 4.2 \times 10^{-14}$ cm^2 s^{-1}. This value is similar to that obtained [97] by the light scattering technique for the phase separation of PMMA/PVAc blends.

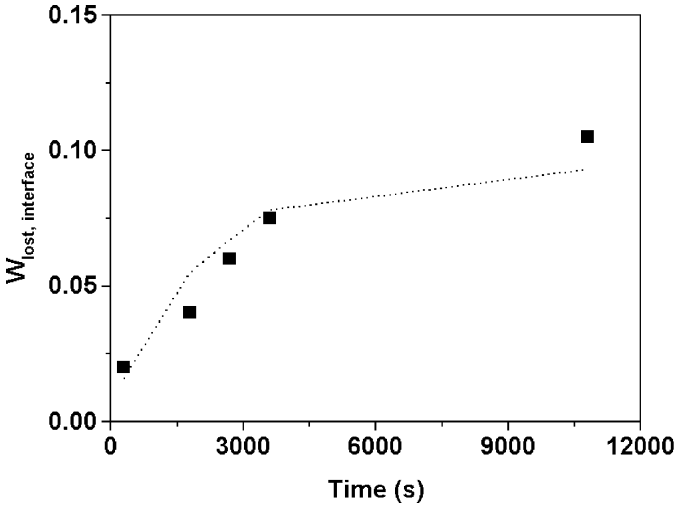

Figure 3.45. Weight fraction of PMMA which has diffused into the core phase versus annealing time at 150°C. [Dotted line is Eq. (41)].

4.4 MORPHOLOGY ANALYSIS OF INTERPENETRATING POLYMER NETWORKS

An interpenetrating polymer network (IPN) is defined as a combination of two crosslinked polymers, at least one of which has been synthesised [98] and/or crosslinked in the immediate presence of the other. From the topological point of view, IPNs are closely related to polymer blends and to block, graft and crosslinked copolymers. From the synthesis point of view, IPNs can be classified, broadly, into two general types: (a) sequential IPNs where a polymer network is formed which is then swollen by the monomer, plus a crosslinking agent and an activator, which is then polymerised in situ to form the second network; and (b) simultaneous IPNs (SIPN) where the components necessary to form both networks are mixed and polymerised, at the same time, by non-competing mechanisms. If one of the two polymers is linear (uncrosslinked), a semi-IPN results. A homo-IPN results if both the network polymers are identical in chemical composition [98].

Since the second polymer is still in monomeric form when it is mixed with the first polymer, there is still a considerable entropy of mixing and many monomer–polymer combinations are possible. Upon polymerisation, however, the entropy of mixing is greatly decreased and phase separation [98] usually occurs. The vast majority of IPNs are phase separated multiphase materials. The networks limit the extent of phase separation and give a degree of control of the phase size and extent of mixing of the two components.

Since the historic synthesis of an IPN by Millar [99] in 1960, many papers, including reviews, on IPNs, have been published, and around 20 different products are offered on the market [100]. Most of the papers describe the synthesis and morphological behaviour [98,101–109], status and developments [110,111], properties [112] and industrial applications [113–116] and self-organisation [117] of IPNs. In recent years, a significantly increasing number of commercial IPN products ranging from false teeth to ion-exchange resins, high impact plastics, thermoplastics, adhesives, vibration damping materials and high temperature alloys have been developed.

It is often important to know the morphology of IPNs and the factors influencing it, since phase size, shape and connectivity and the nature of the interphase boundary determine the physical and mechanical properties of such materials. Together, these parameters combine to describe the morphology of the IPN. IPN morphology can be particularly complicated and has been the subject of many studies [118,119]. Most show that during polymerisation, two competing processes take place simultaneously. Phase separation of the forming polymer chains proceeds by diffusion through

an increasingly viscous medium to form the domains. The formation of crosslinks restricts this diffusion and, at gelation, the then present situation is frozen in. Consequently, phase separation in IPNs depends primarily on (i) the miscibility of the constituent polymers, (ii) the crosslink density in both polymer networks and any inter-network grafting, (iii) the reaction conditions (temperature, pressure) and (iv) the relative reaction rates of network formation. With highly incompatible polymers, the thermodynamic driving force for phase separation is so powerful that gross phase separation occurs before gelation [98].

Among the techniques that have been used to investigate IPN morphology are DSC [16,120], TEM [121], SEM [122], DMTA [19], SANS [29], SAXS [123] and dielectric measurements [124]. Inevitably there have been disagreements about the levels of miscibility in particular systems. The reader who wants further background should refer to Refs. [125–127]. To address this problem of the degree of mixing in IPNs, there is a continuing need for new techniques. Two approaches reported recently by Meyer co-workers [128] and Winnik *et al.* [129] involve solid-state NMR spin-diffusion [128] and direct non-radiative energy transfer [130] experiments, respectively. Can the MTDSC developments already introduced in this chapter play a role in revealing, in more detail, the morphologies of IPNs?

4.4.1 Characterisation of Glass Transition Behaviour in Interpenetrating Polymer Networks

The multi-phase nature of IPNs results in complicated glass transition behaviour [101]. Figure 3.46 shows that heat capacity changes with temperature for a series 60:40 polyurethane (PU)/ polystyrene (PS) IPNs (see Table 3.5 for the compositional details) [131,132]. It is, however, not possible to obtain much detailed information from these heat capacity signals.

Figures 3.47(a)–(e) show dC_p/dT versus temperature data for IPN2, IPN3, IPN4, IPN6 and IPN8. The dC_p/dT signal is much more sensitive to the transitions. Figure 3.48 gives a comparison of the dC_p/dT versus temperature plots of a 40% PS + 60% PU physical blend, a situation where no interphase can exist, and IPN9. It is obvious from these figures that the morphologies of these samples are quite complex. The transition region is very broad covering a span of about 180°C. For IPN4 and IPN8, there are broad transitions from 20 to 120°C [131,132].

The crosslink density in the PU component in this series of IPNs was varied by changing the diol/triol ratio. The crosslink level and the glass transition temperature, obtained via MTDSC, are listed in Table 3.6.

It can be seen that with increasing crosslink density in the PU network, the PU T_g shifted towards higher temperature. Figure 3.47 shows that not

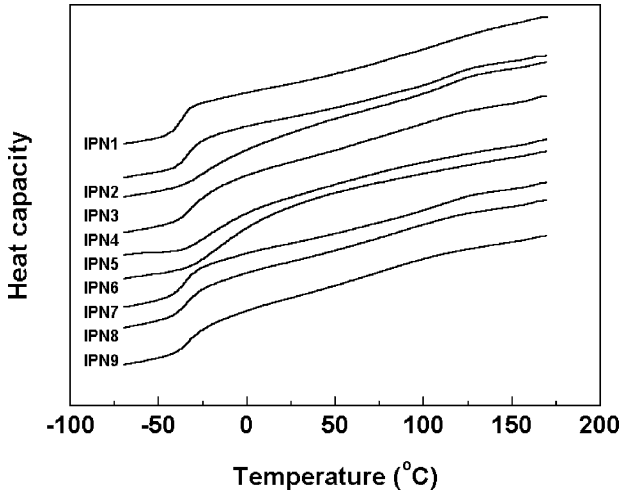

Figure 3.46. Heat capacity versus temperature data for IPN1 to IPN9.

only did the peak location change to higher temperature, but also that the peak decreased in height, and, simultaneously, became broader. The PS transition remained at the same location.

These samples, simultaneous PU/PS IPNs, were synthesised by a one-short route. The IPN topology appears to restrict phase separation, which results in materials with broad transition regions. By variation of the crosslink level in either or both polymer networks, the controlled introduction of inter-network grafting or the incorporation of compatibilisers into the PS network, the compatibility of the two polymer networks can be increased. For simultaneous IPNs, it has been found [129] that the network which is first formed

Table 3.5. Composition of the PU/PS IPN series

Code	PU/PS	Diol/triol	DVB[a]
IPN1	60/40	7:1	5 mol%
IPN2	60/40	3:1	5 mol%
IPN3	60/40	1:1	5 mol%
IPN4	60/40	3:1	5 mol% with 1 wt% of TMI[b]
IPN5	60/40	3:1	5 mol% with 5 wt% of TMI[b]
IPN6	60/40	3:1	5 mol% with 10 wt% of TMI[b]
IPN7	60/40	3:1	5 mol% standard polymerisation
IPN8	60/40	3:1	5 mol% with 10 wt% of compatibiliser[c]
IPN9	60/40	3:1	5 mol% with 2.5 wt% of TMI

[a] DVB: divinybenzene.

[b] TMI: benzene-1-(1-isocyanato-1-methylethyl)-3-(1-methylethenyl).

[c] Compatibiliser: a polyoxypropylene glycol 1025 molecule terminated at both ends with TMI units is incorporated in the PS network.

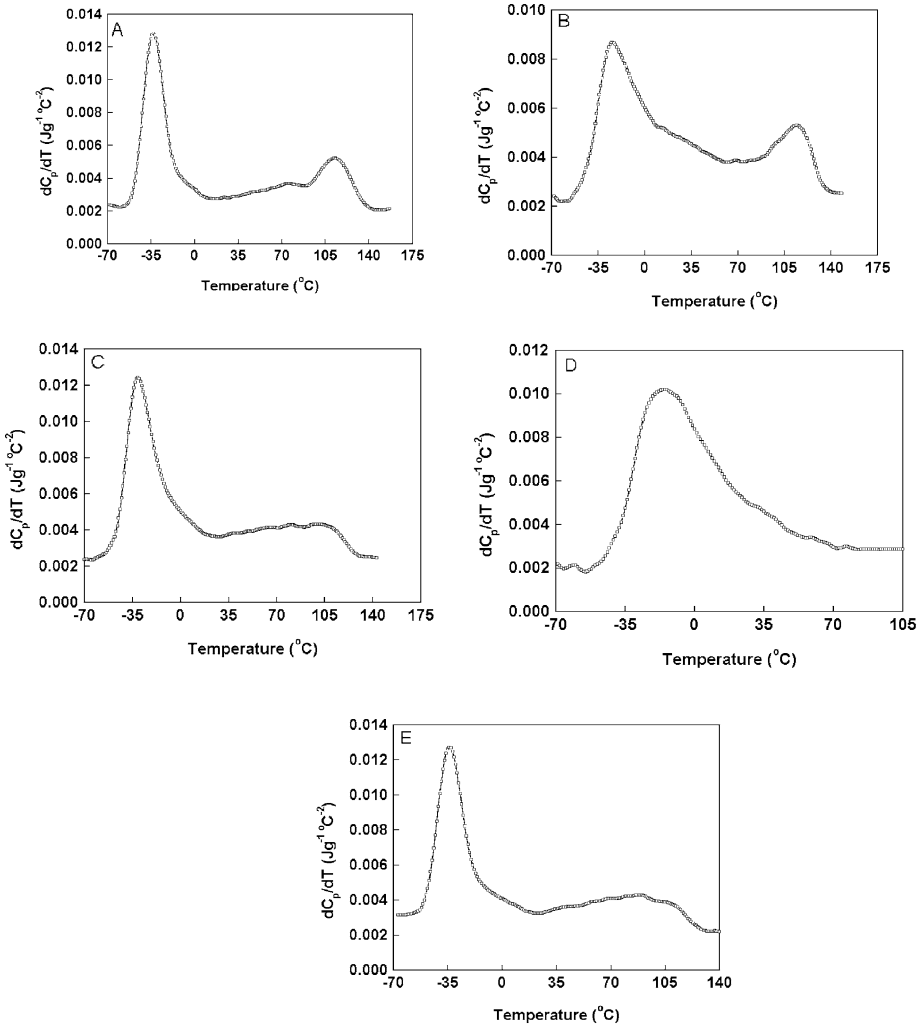

Figure 3.47. dC_p/dT versus temperature data for (A) IPN2, (B) IPN3, (C) IPN4, (D) IPN6 and (E) IPN8.

represents the continuous phase. Hourston and Schafer [133,134] investigated the rate of network formation in the 60:40 PU/PS IPN (IPN7) by means of FTIR spectroscopy coupled with a heated cell unit. The conversion curves of both networks were monitored by following integrated peak areas versus time. This study confirmed that under the given reaction conditions, the PU network formed first. In such a situation, it is believed that several possible morphologies could result. (a) The two networks could be miscible yielding

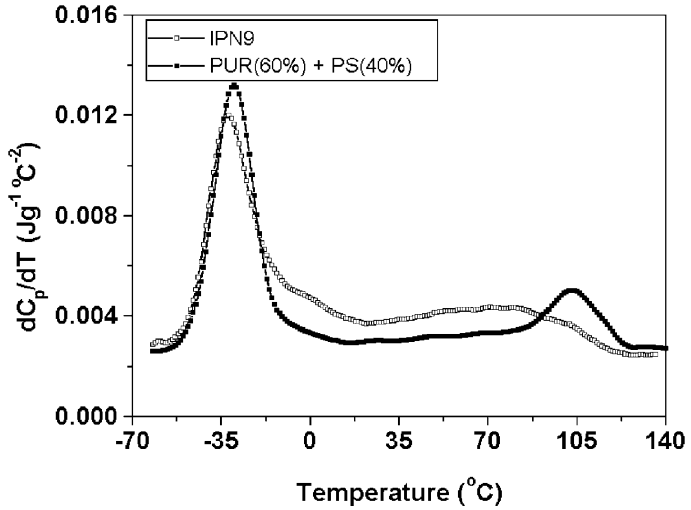

Figure 3.48. dC_p/dT versus temperature data for the 40% PS + 60% PUR physical blend and for IPN9.

a homogeneous material. (b) The first-formed network could be uniformly distributed in space, but with the second-formed network heterogeneously distributed. (c) Both networks could be heterogeneously distributed in space, but with interfacial zones containing a mixture of the two networks. For the first situation, a single glass transition would be obtained. For the second situation, the glass transition temperatures could be shifted somewhat. For the third situation, the glass transition region will broaden.

4.4.2 Model Experiment

The aim is to establish a quantitative analysis method applicable to IPNs. A spectrum can be synthesised by using an analogue method to sum a series of functions representing individual peaks in order to produce a final function that closely represents the experimental spectrum.

Table 3.6. Crosslink level and glass transition temperatures

		T_g (°C)[a]	
Diol/triol	**DVB**	**PU-rich phase**	**PS-rich phase**
7:1(IPN1)	5 mol%	−38	113
3:1(IPN2	5 mol%	−33	113
1:1(IPN3)	5 mol%	−24	113

[a] The T_g values were obtained by the multi-peak resolution technique (133,134).

For an IPN, we may consider dC_p/dT as a multiple Gaussian function in the glass transition region.

$$
\begin{aligned}
dC_p/dT &= B + f(T) \\
f(T) &= \sum_i f_i(T, T_{gi}, \omega_{di}, \Delta C_{pi}) \\
&= \Delta C_{p1}/[\omega_{d1}(\pi/2)^{1/2}]\exp\left[-2(T - T_{g1})^2/\omega_{d1}^2\right] \\
&\quad + \Delta C_{p2}/[\omega_{d2}(\pi/2)^{1/2}]\exp\left[-2(T - T_{g2})^2/\omega_{d2}^2\right] \\
&\quad + \Delta C_{p3}/[\omega_{d3}(\pi/2)^{1/2}]\exp\left[-2(T - T_{g3})^2/\omega_{d3}^2\right] \\
&\quad + \cdots
\end{aligned} \tag{42}
$$

where $f_i(T)$ is related to the ith phase of the multi-phase system.

To evaluate this model, an experiment with a four-component system was conducted This system was a poly(methyl acrylate)/poly(vinyl acetate) (PMA/PVAc) physical blend, or mixture, consisting of four individual blends (PMA/PVAc (80/20) + PMA/PVAc (60/40) + PMA/PVAc (40/60) + PMA/PVAc (20/80)). PMA is miscible with PVAc. The open squares in Figure 3.49 are the experimental dC_p/dT data. The difference between glass transition temperatures of PMA and PVAc is about 33°C. In the glass transition region, the four-component mixture showed an acceptable fit to the experimental data, see Figure 3.49. The solid lines shown in Figure 3.49

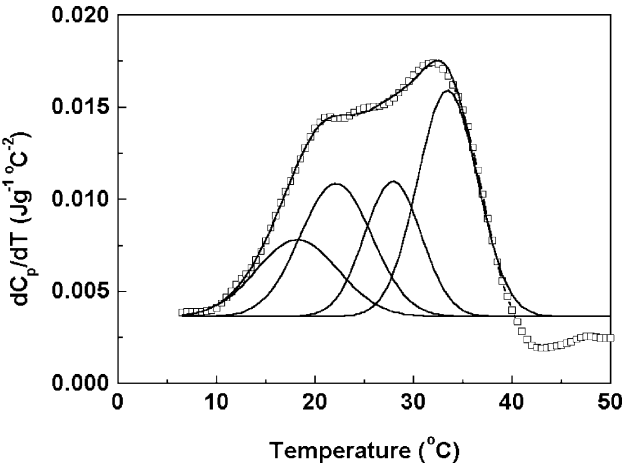

Figure 3.49. Comparison of experimental data with peak resolution results for a four-component model system.

Table 3.7. Comparison of known weight fraction with the calculated value

System	Known	Calculated
PMA-20	30	27.8
PMA-40	23	21.1
PMA-60	25	22.9
PMA-80	22	19.7

are the fitting and peak resolution results. The conditions for the fitting and peak resolution are as follows.

1: ΔC_p (fitting) = ΔC_p (experimental).

2: $\Delta T_g = w_1 \Delta T_{g1} + w_2 \Delta T_{g2}$.

ΔT_g is the transition width and ΔT_{g1} and ΔT_{g2} are the glass transition widths for pure polymer 1 and polymer 2, respectively. Table 3.7 shows the comparison of the known and calculated results. The average difference is about 8%.

Curve fitting of this type assumes that a particular peak profile is uniquely characterised once its peak width at half maximum has been fixed, and cannot be resolved into sub-components. In most practical situations, a Gaussian profile is unique and curve fitting may be undertaken [135].

4.4.3 Analysis of Phase Structure of IPNs

Consider that there exist interfacial phases in IPNs. The dC_p/dT signal may then be divided into three parts by the peak resolution method. These are related to the PU-rich, PS-rich and the interfacial phases. The phase that has the lowest T_g is considered as a PU-rich phase and the phase with the highest T_g is considered as being PS-rich. Other phases located between the PU-rich and PS-rich phases are considered as being interfacial.

As examples, Figure 3.50 shows the peak resolution results [131] for the IPN1, IPN2, IPN7, IPN8 and IPN9 materials discussed above.

For IPN1, three transition peaks were obtained. For IPN2, IPN7, IPN8 and IPN9, four transition peaks were involved. DMTA measurements [134] showed that the glass transition temperatures of the PS-rich phase in the IPN1, IPN2 and IPN3 were the same, 133°C. The original MTDSC data for IPN1, IPN2 and IPN3 showed that the glass transition temperatures of the PS-rich phase were different. However, the peak resolution results give the same glass transition temperature, 113°C, for the PS-rich phase in the IPN1, IPN2 and IPN3 materials. The difference may result from the effect of the interface, which results in the shift and broadening of the dC_p/dT peak.

Table 3.8 gives the results of this analysis for the IPN1, IPN2, IPN8 and IPN9 materials.

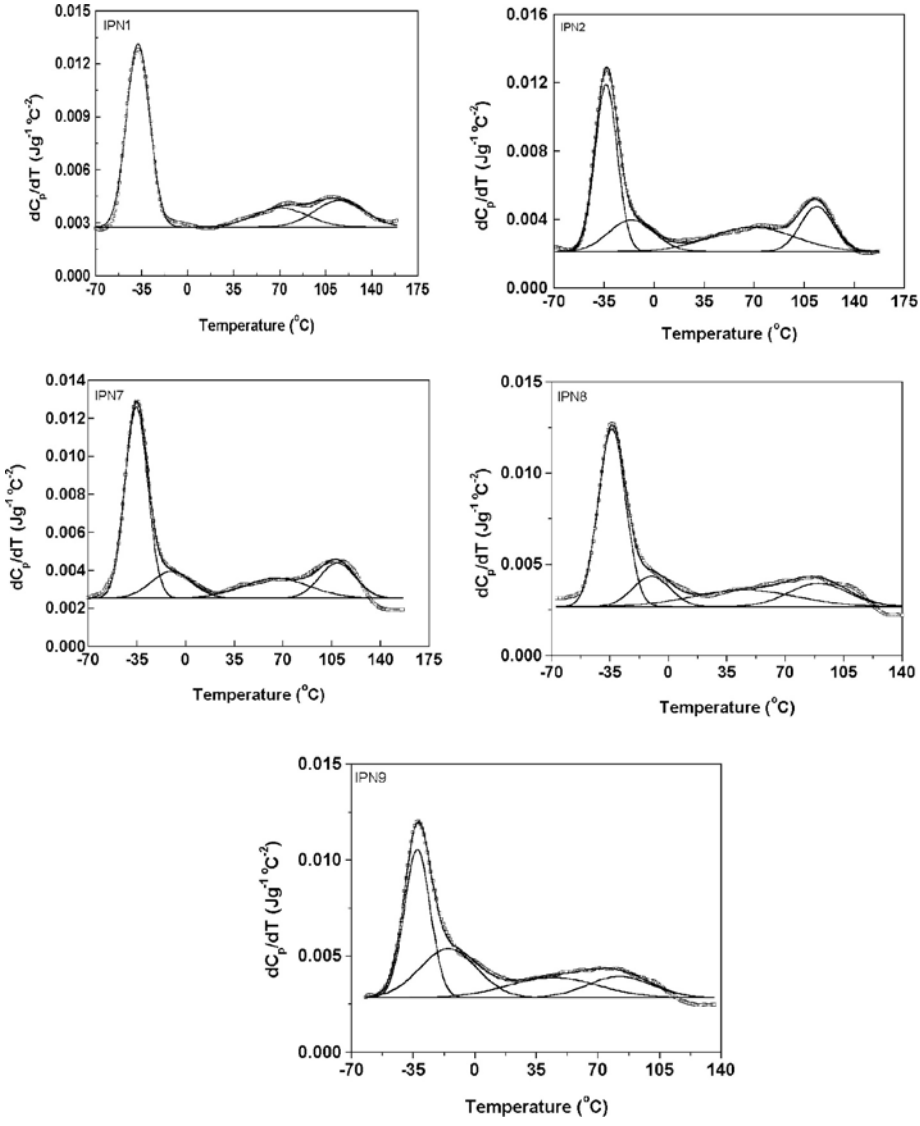

Figure 3.50. Comparison of experimental dC_p/dT data with peak resolution results for the IPN1, IPN2, IPN7, IPN8 and IPN9 materials.

From Table 3.8, it can be seen that there are several different levels of network compatibility. For IPN8, there are PU-rich phases whose T_gs are located at about −33, and −10°C, and PS-rich phases whose T_gs are located at about 46 and 88°C, respectively. For IPN9, there are PU-rich phases at about −33 and −17°C, and PS-rich phases at about 50 and 90°C, respectively. The total interface content in IPN8 and IPN9 is high. This

Table 3.8. T_g and weight fraction values for the IPNs [131]

System	T_g (°C)	Weight fraction (%)
IPN1	−38	58
	70	14 interface
	113	30
IPN2	−33	48
	−15	16 interface
	70	15 interface
	113	20
IPN8	−33	43
	−10	17 interface
	46	20 interface
	88	21
IPN9	−33	32
	−17	23 interface
	50	30 interface
	90	19

correlates well the high loss peak in the DMTA data [134]. For IPN2, there are PU-rich phases whose T_g is located at about −15°C and PS-rich phases whose T_g is at about 70°C. In the PU-rich phases, the weight fraction of PS is about 18% and in the PS-rich phases, the weight fraction of PU is about 24%.

By combining the TEM and MTDSC techniques, a clearer understanding of the morphology of IPNs may be obtained. From TEM measurements, phase domain size and shape and connectivity can be determined. From MTDSC measurements, the weight fraction of interphase regions can be obtained. So, the relationships between mechanical properties and IPN morphology can now, in practice, be more comprehensively investigated.

5 Conclusions

It has been shown in this chapter that the MTDSC technique is a very useful tool in the study of several aspects of polymer blends and related materials including structured latexes and interpenetrating polymer networks. It is important to note that the dC_p/dT versus temperature signal may be used not only qualitatively as a sensitive detector of transitions impossible to spot by other thermal techniques such as conventional DSC and DMTA, but it may also be used to significant advantage in a quantitative way. It has been shown that it is sensitive to the diffuse interface between phases. Thus, from dC_p/dT versus temperature signals, the weight fraction of the diffuse interface can be quantified. There are many situations where this will prove to be very valuable.

References

[1] B.J. Hunt and M.I. James, Polymer Characterisation, Blackie Academic & Professional, London, (1993).
[2] L.H. Sperling, Introduction to Physical Polymer Science, John Wiley & Sons, Inc, NY (1992).
[3] S.L. Cooper and G.M. Estes, Multiphase Polymers, American Chemical Society, Washington, DC (1979).
[4] J.A. Manson and L.H. Sperling, Polymer Blends and Composites, Plenum Press, NY (1976).
[5] O. Olabisi, L. Robeson and M.T. Shaw, Polymer–Polymer Miscibility, Academic Press, NY (1979).
[6] D.R. Paul and S. Newman, Polymer Blends, Academic Press, London (1978).
[7] G.D. Spathis, E.P. Sideridis and P.S. Theocaris, Int. J. Adhes. Adhes., 1 (1981) 195.
[8] P.S. Theocaris and G.D. Spathis, J. Appl. Polym. Sci., 27 (1982) 3019.
[9] J. Koberstein, T. Morra and R.S. Stein, J. Appl. Crystallogr., 13 (1980) 34.
[10] F. Annighofer and W. Gronski, Makromol. Chem., 185 (1984) 2231.
[11] R.J. Roe, J. Appl. Crystallogr., 15 (1982) 18.
[12] F. Annighofer and W. Gronski, Colloid Polym. Sci., 261 (1983) 15.
[13] A.C. Fernandes, J.W. Barlow and D.R. Paul, J. Appl. Polym. Sci., 32 (1986) 6073.
[14] A.C. Fernandes, Ph.D. Dissertation, University of Texas, Austin (1986).
[15] M.J. Folkes and P.S. Hope, Polymer Blends and Alloys, Chapman and Hall, London, (1993).
[16] S. Singh, H.L. Frisch and H. Ghiradella, Macromolecules, 23 (1990) 375.
[17] M. Annakutty and P.C. Deb, J. Appl. Polym. Sci., 45 (1992) 2145.
[18] H.R. Allcock, K.B.Visscher and I. Manners, Chem. Mater., 4 (1992) 1188.
[19] Y. Lipatov, V.F. Rosovizky, P.V. Datsko and Y. Maslak, J. Appl. Polym. Sci., 36 (1988) 1143.
[20] D. Vesely, In Polymer Blends and Alloys, M.J. Folkes and P.S. Hope, Eds., Blackie Academic & Professional, London (1993).
[21] K. Kato, Polym. Eng. Sci., 1 (1967) 38.
[22] D.A. Thomas, In Advances in Preparation and Characterisation of Multi-polymer Systems, R.J. Ambrose and S.L. Aggarwal, Eds., John Wiley and Sons, NY (1978).
[23] W. Ruland, Macromolecules, 20 (1987) 87.
[24] T. Nishi, T.T. Wang and T.K. Kwei, Macromolecules, 8 (1975) 277.
[25] M. Song, H. Liang, Y. Chen and B. Jiang, Acta Phys. Chem. Sin., 5 (1991) 513.
[26] V. Nelliappan, M.S. El-Aasser, A. Kilein, E.S. Daniels and J.E. Roberts, J. Appl. Polym. Sci., 58 (1995) 323.
[27] M. Hidalgo, J. Guillot, M.F. Llauro and H Waton, J. Chem. Phys., 89 (1992) 505.
[28] G. Krause and K.W. Rollmann, J. Polym. Sci. Polym. Phys., 14 (1976) 1133.
[29] B. McGarey, In Advances in Interpenetrating Polymer Networks, D. Klempner, K.C. Frisch, Eds. Technomic Publishing Co., Lancaster (1989) p. 69.
[30] M. Song, D.J. Hourston, F.-U. Schafer, H.M. Pollock and A. Hammiche, Thermochim. Acta, 315 (1998) 25.
[31] D.J. Hourston, M. Song, H.M. Pollock and A. Hammiche, J. Thermal Anal., 49 (1997) 209.
[32] D.J. Hourston, M. Song, A. Hammiche, H.M. Pollock and M. Reading, Polymer, 38 (1997) 1.
[33] R.F. Boyer, J. Macromol. Sci. B, 7 (1973) 487.

[34] M.J. Richardson and N.G. Savill, Polymer, 16 (1975) 753.
[35] B. Wunderlich, Thermal Analysis, Academic Press, Boston (1990).
[36] B. Wunderlich and L.D. Jones, J. Macromol. Sci. B, 3 (1969) 67.
[37] B. Wunderlich, Polymer Handbook, Published by John Wiley & Sons New York, Second Edition Section V-55 (1992).
[38] M. Song, A. Hammiche, H.M. Pollock, D.J. Hourston and M. Reading, Polymer, 37 (1996) 5661.
[39] M. Song, A. Hammiche, H.M. Pollock, D.J. Hourston and M. Reading, Polymer, 36 (1995) 3313.
[40] A.K. Nandi, B.M. Mandal and S.N. Bhattacharyya, Macromolecules, 18 (1985) 1454.
[41] P. Perrin and R.E. Prud'homme, Polymer, 32 (1991) 1468.
[42] X. Lu and R.A. Weiss, Macromolecules, 25 (1992) 3242.
[43] J.N. Clark, J.S. Higgins, C.K. Kim and D.R. Paul, Polymer, 33 (1992) 3137.
[44] M. Song, H.M. Pollock, A. Hammiche, D.J. Hourston and M. Reading, Polymer, 38 (1997) 503.
[45] S. Wu, Polymer Interfaces and Adhesion, Dekker, NY (1982).
[46] G. Helfand and Y. Tagami, J. Chem. Phys., 56 (1972) 3592.
[47] K.M. Hong and J. Noolandi, Macromolecules, 15 (1982) 482.
[48] C.I. Poser and I.C. Sanchez, Macromolecules, 24 (1984) 79.
[49] N.H. Sung, A. Kaul, I. Chin and C.S.P. Sung, Polym. Eng. Sci., 22 (1982) 637.
[50] K. Binder and H. Sillescu, In Encyclopedia of Polymer Science and Engineering, Vol. 20, Wiley, NY (1989) p. 297.
[51] H.H. Kausch and M. Tirrell, Ann. Rev. Mater. Sci., 19 (1989) 341.
[52] T.K. Kwei and T.T. Wang, In Polymer Blends, Vol. 1, D.R. Paul and S. Newman, Eds., Academic, NY (1978) pp. 141–185.
[53] H. van Oene, In Polymer Blends, Vol. 1, D.R. Paul and S. Newman, Eds., Academic, NY (1978).
[54] S. Wu, presented at 16th Europhysics Conference on Macromolecules, Polymer Alloys: Structure and Properties, Brugge, Belgium (1984).
[55] Y.H. Kim and R.P. Wool, Macromolecules, 16 (1983) 1115.
[56] K. Judd, H.H. Kausch and J.W. Williams, J. Mater. Sci., 16 (1981) 204.
[57] C.D. Han, Multiphase Flow in Polymer Processing, Academic Press, NY (1981).
[58] P.T. Gilmore, R. Falabella and R.L. Laurence, Macromolecules 13 (1980) 880.
[59] G. Fytas, Macromolecules, 20 (1987) 1430.
[60] S.S. Voyutskii, Adhesion, 3 (1971) 69.
[61] J.K. Kim and C.D. Han, Polym. Eng. Sci., 31 (1991) 258.
[62] P.F. Green and B.L. Doyle, Macromolecules, 20 (1987) 2471.
[63] F. Brochard-Wyart and P.G. de Gennes, Makromol. Chem. Makromol. Symp., 40 (1990) 167.
[64] F. Brochard-Wyart, Proc. Toyota Conf. Stud. Polym. Sci., 2 (1988) 249.
[65] A. Brochard-Wyart and P. Pincus, C. R. Acad. Sci. Ser. II, 314 (1992) 131.
[66] E. Jabbari and N.A. Peppas, Macromolecules, 26 (1993) 2175.
[67] P.G. de Gennes, C. R. Acad. Sci. Ser. II, 292 (1981) 1505.
[68] F. Brochard-Wyart, J. Jouffroy and P. Levinson, Macromolecules, 16 (1983) 1638.
[69] P.G. de Gennes, J. Chem. Phys., 72 (1980) 4656.
[70] S.F. Tead and E.J. Kramer, Macromolecules, 21 (1988) 1513.
[71] P.F. Green, C.J. Palmstrom, J.W. Mayer and E.J. Kramer, Macromolecules, 18 (1985) 501.
[72] E.J. Kramer, P.F. Green and C.J. Palmstrom, Polymer, 25 (1984) 473.
[73] H. Sillescu, Makromol. Chem. Rapid Commun., 8 (1987) 393.

[74] A.Z. Akcasu, G. Nagele and R. Klein, Macromolecules, 24 (1990) 4408.
[75] J.V. Seggern, S. Klotz and H.J. Cantow, Macromolecules, 22 (1989) 3328.
[76] E.A. Jordan, R.C. Ball, A.M. Donald, L.J. Fetters, R.A.L. Jones and J. Klein, Macromolecules, 21 (1988) 235.
[77] G. Reiter, S. Huttenbach, M. Foster and M. Stamm, Macromolecules, 24 (1991) 1179.
[78] S. Wu, H.K. Chuang and C.D. Han, J. Polym. Sci. Polym. Phys., 24 (1986) 143.
[79] E. Kim, E.J. Kramer, W.C. Wu and P.D. Garrett, Polymer, 35 (1994) 5706.
[80] P.G. de Gennes, Scaling Concepts in Polymer Physics, Cornell University Press, Ithaca, NY (1979).
[81] S. Prager and M.J. Tirrell, Chem. Phys., 75 (1981) 5194.
[82] S. Prager, D. Adolf and M. Tirrell, J. Chem. Phys., 78 (1983) 7015.
[83] D.B. Adolf, Macromolecules, 17 (1984) 1248.
[84] J. Crank, The Mathematics of Diffusion, Oxford University Press, London (1975).
[85] U. Murschall, E.W. Fischer, C.H. Herkt-Maetzky and G. Fytas, J. Polym. Sci. Polym. Lett., 24 (1986) 193.
[86] P.T. Gilmore, R. Falabella and R.L. Laurence, Macromolecules, 13 (1980) 880.
[87] M.A. Winnik, Y. Wang and F. Haley, J. Coating Technol., 64 (1992) 51.
[88] M. Chainey, M.C. Wilkinson and J. Hearn, J. Polym. Sci. Polym. Chem., 23 (1985) 2947.
[89] O. Pelcan, Trends Polym. Sci., 2 (1994) 236.
[90] Y. Wang and M.A. Winnik, Macromolecules, 23 (1990) 4731.
[91] M.C. Goh, D. Juhue, O.M. Leung, Y. Wang and M.A.Winnik, Langmuir, 9 (1993) 1319.
[92] M. Song, D.J. Hourston, H.X. Zhang, H.M. Pollock and A. Hammiche, Polymer, 42 (2001) 6299.
[93] D. Juhue and J. Lang, Macromolecules, 28 (1995) 1306.
[94] F. Lin and D.J. Meier, Langmuir, 11 (1995) 2726.
[95] D.J. Hourston, H.X. Zhang, M. Song, H.M. Pollock and A. Hammiche, Thermochim. Acta, 294 (1997) 23.
[96] J. Brandrup and E.H. Immergut, Eds., Polymer Handbook, John Wiley & Sons, NY (1966).
[97] M. Song, Y. Huang, G. Cong, H. Liang and B. Jiang, Polymer, 33 (1992) 1293.
[98] L.H. Sperling, Interpenetrating Polymer Networks and Related Materials, Plenum Press, NY (1981).
[99] J.H. Saunders and K.C. Frisch, Polyurethane-Chemistry and Technology, Interscience, New York (1964).
[100] L.H. Sperling, In Advance Interpenetrating Polymer Networks, Vol. 4, D. Klempner and K.C. Frisch, Eds., Technomic, Lancaster, PA (1994) p. 1.
[101] L.H Sperling, Contemp. Top. Polym. Sci., 6 (1989) 665.
[102] Y. Lipatov, S.V.V. Shilov, V.A. Bogdanovic, L.V. Karabanova and L.M. Sergeeva, J. Polym. Sci. Polym. Phys., 25 (1987) 43.
[103] D.J. Hourston and Y. Zia, J. Appl. Polym. Sci., 28 (1983) 3849.
[104] D.J. Hourston and Y. Zia, J. Appl. Polym. Sci., 28 (1983) 3745.
[105] Y. Lipatov, V.F. Rosovizky, P.V. Datsko and Y. Maslak, J. Appl. Polym. Sci., 36 (1988) 1143.
[106] B. Suthar, N. Parikh and N. Patel, Polym. Int., 25 (1991) 173.
[107] D.J. Hourston and Y. Zia, J. Appl. Polym. Sci., 29 (1984) 2963.
[108] D.J. Hourston and Y. Zia, J. Appl. Polym. Sci., 30 (1985) 2157.
[109] D.J. Hourston and S. Decurtins, J. Appl. Polym. Sci., 36 (1988) 365.
[110] L.H. Sperling, J.J. Fay, C.J. Murphy and D.A. Thomas, Makromol. Chem. Makromol. Symp., 38 (1990) 99.

[111] B. Suthar, In Advances in Interpenetrating Polymer Networks, Vol. 2, D. Klempner and K.C. Frisch, Ed., Technomic, Lancaster, PA (1990) 281.
[112] L.H. Sperling and J.J. Fay, Polym. Adv. Technol., 2 (1991) 44.
[113] Y. Suzuki, Nippon Gomit Kyokaishi, 62 (1989) 593.
[114] J. Qin, F. Li, Z. Wu and B. Cian, In Advance Interpenetrating Polymer Networks, Vol. 2, D. Klempner and K.C. Frisch., Eds., Technomic, Lancaster, PA (1990) 205.
[115] T. Akio and H. Mizunachi, In Advances in Interpenetrating Polymer Networks, Vol. 3, D. Klempner and K.C. Frisch, Eds., Technomic, Lancaster, PA (1991) 25.
[116] L.H. Sperling, C.E. Carraher, S.P. Qureshi, J.A. Manson and L.W. Barret, In Biotechnol. Polym. (Proc. Am. Chem. Soc. Symp.), C.G. Gebelein, Ed., Plenum Press, New York (1990) p. 96.
[117] Y. Lipatov, Rev. Macromol. Chem. Phys., C30 (1990) 209.
[118] J.H. An and L.H. Sperling, In Cross-Linked Polymers, R.A. Dickie, S.S. Labana and R.S. Bauer, Ed., ACS Series 376, American Chemical Society, Washington DC (1988).
[119] D. Klempner and H. Berkowski, In Encyclopedia of Polymer Science and Engineering, Vol. 8, H. Mark, N.M. Bikales, C.G. Overberger and G. Menges, Ed., John Wiley & Sons, NY (1988).
[120] H.L. Frisch, D. Klempner, H.K.Yoon and K.C. Frisch, Macromolecules, 13 (1980) 1016.
[121] D.J. Hourston, F.-U. Schafer, J.S. Bates and M.H.S. Gradwell, Polymer, 39 (1998) 3311.
[122] M. Akay and S.N. Rollins, Polymer, 34 (1993) 1865.
[123] S. Ma, Synthesis and Characterisation of Interpenetrating Polymer Networks, Ph.D. Thesis, Jilin University, People's Republic of China (1988).
[124] A. Alig, M. Junker, W. Jenninger, H.L. Frisch and M. Schulz, Morphology of Polymers, Conference lecture, Prague, July 1995.
[125] M.M. Coleman, C.J. Serman and P.C. Painter, Macromolecules, 20 (1987) 226.
[126] B.J. Bauer, R.M. Briber and C.C. Han, Macromolecules, 22 (1989) 940.
[127] B.J. Bauer and R.M. Briber, In Advances in Interpenetrating Polymer Networks, Vol. 4, D. Klempner and K.C. Frisch, Ed., Technomic, Lancaster, PA (1994) p. 45.
[128] N. Parizel, G. Meyer and G. Well, Polymer, 36 (1995) 2323.
[129] A.A. Donatelli, L.H. Sperling and D.A. Thomas, J. Appl. Polym. Sci., 21 (1977) 1189.
[130] Y. Yang, M.K. Winnik, D. Ylitalo and R.J. Devoe, Macromolecules, 29 (1996) 7055.
[131] M. Song, D.J. Hourston, F.-U. Schafer, H.M. Pollock and A. Hammiche, Thermochim. Acta, 305 (1997) 335.
[132] M. Song, D.J. Hourston, F.-U. Schafer, H.M. Pollock and A. Hammiche, Thermochim. Acta, 315 (1998) 25.
[133] D.J. Hourston and F.-U. Schafer, J. Polym. Adv. Technol., 7 (1995) 273 (special edition).
[134] F.-U. Schafer, Ph.D. thesis, Loughborough University (1996).
[135] A. Baruya and W.F. Maddams, Appl. Spectrosc., 32 (1978) 563.